EJN fens European Journal of Neuroscience

European Journal of Neuroscience, Vol. 30, pp. 1036–1055, 2009 doi:10.1111/j.1460-9568.2009.06896.x

NEUROSYSTEMS

Lack of kainic acid-induced gamma oscillations predicts subsequent CA1 excitotoxic cell death

Seiichiro Jinde,[1,*] Juan E. Belforte,[1,†] Jun Yamamoto,[2] Matthew A. Wilson,[2] Susumu Tonegawa,[2,3] and Kazu Nakazawa[1]

[1]Unit on the Genetics of Cognition and Behavior, Mood and Anxiety Disorders Program, National Institute of Mental Health, National Institutes of Health, Department of Health and Human Services, MD 20892, USA

[2]The Picower Institute for Learning and Memory, RIKEN-MIT Center for Neural Circuit Genetics, Massachusetts Institute of Technology, Cambridge, MA 02139, USA

[3]Howard Hughes Medical Institute, Massachusetts Institute of Technology, Cambridge, MA 02139, USA

Keywords: CA3, epilepsy research, GABA, mouse, NMDA receptors

Abstract

Gamma oscillations are a prominent feature of hippocampal network activity, but their functional role remains debated, ranging from mere epiphenomena to being crucial for information processing. Similarly, persistent gamma oscillations sometimes appear prior to epileptic discharges in patients with mesial temporal sclerosis. However, the significance of this activity in hippocampal excitotoxicity is unclear. We assessed the relationship between kainic acid (KA)-induced gamma oscillations and excitotoxicity in genetically engineered mice in which *N*-methyl-D-aspartic acid receptor deletion was confined to CA3 pyramidal cells. Mutants showed reduced CA3 pyramidal cell firing and augmented sharp wave–ripple activity, resulting in higher susceptibility to KA-induced seizures, and leading to strikingly selective neurodegeneration in the CA1 subfield. Interestingly, the increase in KA-induced γ-aminobutyric acid (GABA) levels, and the persistent 30–50-Hz gamma oscillations, both of which were observed in control mice prior to the first seizure discharge, were abolished in the mutants. Consequently, on subsequent days, mutants manifested prolonged epileptiform activity and massive neurodegeneration of CA1 cells, including local GABAergic neurons. Remarkably, pretreatment with the potassium channel blocker α-dendrotoxin increased GABA levels, restored gamma oscillations, and prevented CA1 degeneration in the mutants. These results demonstrate that the emergence of low-frequency gamma oscillations predicts increased resistance to KA-induced excitotoxicity, raising the possibility that gamma oscillations may have potential prognostic value in the treatment of epilepsy.

Introduction

Gamma oscillations in cortical structures, defined as synchronous rhythmic oscillatory activity from 30 to 100 Hz, are believed to play a role in neural communication and information processing (Singer & Gray, 1995; Buzsáki & Draguhn, 2004). Whereas these physiological gamma oscillations are transiently induced by sensory stimulation (for hundreds of milliseconds to 1 s), persistent gamma oscillations lasting for many seconds or even minutes (Traub *et al.*, 1999) have also been observed in human epileptic patients (Uhlhaas & Singer, 2006; Hughes, 2008); indeed, these gamma oscillations are often observed before or coincidently with the onset of seizure discharges (Allen *et al.*, 1992; Fisher *et al.*, 1992; Alarcon *et al.*, 1995; Medvedev, 2001; Jirsch *et al.*, 2006). An increase in high-frequency (60–100-Hz) oscillations prior to the onset of neocortical seizures sometimes anticipates subsequent epileptic seizures (Worrell *et al.*, 2004). In contrast, low gamma oscillations are typically associated with a favorable prognosis after resective surgery (Lee *et al.*, 2000; Park *et al.*, 2002). Therefore, their significance in excitotoxic insults has remained elusive.

Systemic and intrahippocampal injection of kainic acid (KA) in rodents induces epileptiform-like seizures and massive neurodegeneration, which has been used as an animal model of temporal lobe epilepsy (Schwob *et al.*, 1980; Nadler, 1981; Ben-Ari, 1985; Sperk, 1994). Interestingly, KA administration also induces complex epileptiform electroencephalographic patterns, including gamma oscillations, which precede the ictal-like seizure discharges and generalized behavioral seizures (Bragin *et al.*, 1999; Medvedev *et al.*, 2000; Khazipov & Holmes, 2003; Sakatani *et al.*, 2008). KA-induced oscillations in the CA3 subfield of the hippocampus are completely blocked by bicuculline, a γ-aminobutyric acid $(GABA)_A$ receptor antagonist, but they are largely maintained in the presence of the α-amino-3-hydroxy-5-methyl-4-isoxazolepropionic acid receptor antagonists in slice preparations (Fisahn *et al.*, 2004), as well as in *in vivo* preparations (Khazipov & Holmes, 2003). The strong reliance of gamma oscillations on $GABA_A$ receptors suggests that these oscillations arise from a network of mutually connected GABAergic

Correspondence: Dr Kazu Nakazawa, as above.
E-mail: nakazawk@mail.nih.gov

**Present addresess*: Department of Neuropsychiatry, Graduate School of Medicine, The University of Tokyo, 7-3-1 Hongo, Bunkyo-ku, Tokyo 113-8655, Japan

†Department of Physiology, School of Medicine, University of Buenos Aires, Paraguay 2155, 7th floor (1121), Buenos Aires, Argentina

Received 1 April 2009, revised 19 June 2009, accepted 14 July 2009

neurons (Whittington *et al.*, 1995; Bartos *et al.*, 2007; Mann & Paulsen, 2007). KA administration also produces neuronal degeneration, mainly in the limbic area of the brain, where hippocampal pyramidal cells are highly vulnerable (Schwob *et al.*, 1980; Sperk, 1994). However, the relationship between the gamma oscillations that precede seizures and KA-induced excitotoxicity has, to date, not been explored.

In the current study, we initially assessed KA-induced seizure susceptibility in mice where NR1, the essential subunit of *N*-methyl-D-aspartic acid (NMDA) receptors, was selectively ablated from CA3 pyramidal cells [CA3-NR1 knockout (KO) mice, hereafter referred to as mutants] (Nakazawa *et al.*, 2002). We found that, in comparison with control mice, the mutants were more susceptible to KA-induced seizures and massive neurodegeneration, which was confined to area CA1 of the hippocampus. Interestingly, in mutants, persistent 30–50-Hz gamma oscillations prior to seizure discharges were not detectable in area CA1. The relationship between the gamma oscillations that precede seizures and KA-induced excitotoxicity is discussed.

Materials and methods

All experimental procedures were carried out in accordance with the Guide for the Care and Use of Laboratory Animals of the National Research Council, and were approved by the National Institute of Mental Health Animal Care and Use Committee.

Animals

Subjects were naive males of CA3-NR1 KO ($Cre^{+/-}$; $NR1^{flox/flox}$) mutant mice and their three control littermates: floxed-NR1 (fNR1; $Cre^{-/-}$; $NR1^{flox/flox}$), hemizygous G32-4(CA3)-Cre ($Cre^{+/-}$; $NR1^{+/+}$), and wild-type mice from a C57BL/6NTac (B6) background. All mice were between the ages of 18 and 26 weeks, and were obtained by the same breeding method as previously described (Nakazawa *et al.*, 2002). Two to five mice were housed per cage on a 12-h light/dark cycle, with access to food and water *ad libitum*. All of the experiments were conducted by operators who were blind to the mouse genotypes. All animals undergoing seizures or that received the survival surgery for implantation of a microdrive or microwire array were monitored daily for signs of poor health, and any animal that developed moribund poor health was killed. For all the surgeries, anesthesia was induced with i.p. injection of tribromoethanol in tertiary amyl alcohol. Post-operative animals were closely observed and medically treated by the animal care surgeon if necessary.

Behavioral seizure scoring

KA, obtained from Sigma-Aldrich (St Louis, MO, USA) or Tocris Bioscience (Ellisville, MO, USA), was dissolved in 0.9% saline at 5 mg/mL to keep the injection volume below 0.5 mL, and was prepared fresh on the day of each experiment. To establish the optimal dose of KA that induced bilateral forelimb clonus and rearing in about 50% of animals, control fNR1 mice were given intraperitoneal (i.p.) injections of KA, at doses ranging from 15 to 30 mg/kg body weight. Behavioral seizure activity was monitored for 2 h by video camera, and classified according to a modified Racine scale (Racine, 1972): stage 0, normal behavior; stage 1, immobility; stage 2, repetitive movements, myoclonic twitch, or head bobbing; stage 3, bilateral forelimb clonus and rearing; stage 4, continuous rearing and falling; and stage 5, generalized tonic–clonic seizure. Based on the result in Supporting information, Fig. S1, a dose of 20 mg/kg was established to elicit stage 3 seizures in about 40% of fNR1 control mice, with no mortality, and was used throughout the remainder of the experiments. Because no significant score differences were observed when using KA obtained from Sigma-Aldrich or Tocris Bioscience, the data obtained from each drug were combined for this study.

The mutant mice and their three strains of control littermates – fNR1, G32-4-Cre, and B6 – were given i.p. injections of 20 mg/kg KA, and the maximal seizure score was scored every 5 min over the entire 2-h observation period per animal. To evaluate the seizure susceptibility, the latency to stage 3 seizure was measured. If the animal did not show a stage 3 seizure, 120 min was taken as the maximum latency. The occurrence (%) of a stage 4 seizure score and a cumulative seizure score for each animal during the 2-h period were averaged to calculate the rating scale value (± standard error of the mean] for each genotype. In order to evaluate the effect of α-dendrotoxin (DTX), a potent enhancer of presynaptic GABA release, on KA-induced seizures and subsequent events in the mutants, additional experiments were conducted. For instance, various doses of DTX were tested to determine the optimal subconvulsive dose of DTX. An i.p. injection of 0.5 mg/kg body weight induced subconvulsive seizures such as grooming, head nodding, and occasional wet-dog shaking, but no convulsive seizure. Therefore, 0.5 mg/kg was chosen for the subsequent experiments. All of the drugs, except KA from Tocris Bioscience, were purchased from Sigma-Aldrich.

Histological procedures

Mice were deeply anesthetized with tribromoethanol (Avertin; i.p. injection of 0.03 mL of 2.5% tribromoethanol in *t*-amyl alcohol per gram of body weight), and perfused transcardially with 4% paraformaldehyde 1 day, 7 days and 4 weeks after the KA treatment. Untreated animals were used as controls for each genotype. Brains were post-fixed in 4% paraformaldehyde overnight, and 40-μm-thick Vibratome sections were prepared for the following experiments. Our preliminary study showed no significant differences in histological features among the three control genotypes. Therefore, fNR1 mice were chosen as controls for all of the subsequent histological studies. In total, 30 fNR1 mice and 29 mutants were used.

To assess neuronal cellular degeneration, sections were stained with 0.2% Safranin O solution (Polyscience, Inc., Warrington, PA, USA) for Nissl staining. Fluoro-Jade B (Schmued & Hopkins, 2000) and NeuroSilver staining were used to demonstrate perikaryal and terminal degeneration. Fluoro-Jade B staining was performed according to the manufacturer's instruction (Histo-Chem, Inc., Jefferson, AR, USA). Briefly, sections were initially mounted, rehydrated with 80% ethanol and 70% ethanol, washed with distilled water, and incubated in 0.06% potassium permanganate solution for 10 min. The sections were then incubated in 0.0004% Fluoro-Jade B solution containing 0.1% glacial acetic acid for 15 min at room temperature, washed, and mounted with distrene plasticizer xylene (Electron Microscopy Sciences, Hatfield, PA, USA). For silver staining, free-floating 40-μm sections were processed with a silver impregnation protocol according to the manufacturer's instruction (NeuroSilver; FD Neurotechnologies Inc., Baltimore, MD, USA). To evaluate the relationship between behavioral seizure score and excitotoxic injury, the extent of the injury in area CA1 (damage to the CA1 cell layer) was scored on a scale of 0–3, modified from the grading system (Pulsinelli *et al.*, 1982) as a 'damage score', using Nissl staining, as follows: score 0, no injury; score 1, 1–33%; score 2, 34–66%, score 3, 67–100%.

Immunohistochemistry

To evaluate the functional integrity of hippocampal GABAergic neurons, 40-μm-thick parasagittal Vibratome sections were washed

with phosphate-buffered saline (PBS), blocked with 5% normal goat serum in PBS, and incubated at 4 °C with gentle shaking in a monoclonal antibody against the 67-kDa isoform of glutamic acid decarboxylase (GAD67) (1 : 5000; Millipore, Billerica, MA, USA) for three nights. Four sections per animal, which displayed stage 4 or more severe behavioral seizures, were then incubated with Alexa488-conjugated anti-mouse IgG (1 : 200; Molecular Probes, Eugene, OR, USA) at room temperature for 2 h. The numbers of GAD67-positive cells in area CA1, area CA3 and the dentate gyrus (DG) were counted for each section, and the number of positive cells in area CA1 was further counted for each stratum (stratum oriens, pyramidale, stratum radiatum, or stratum lacunosum–moleculare). The cell number was evaluated as a cell density, obtained by dividing the cell number by the area of each subregion/stratum, and was averaged per mouse. For double staining with anti-GAD67 and Fluoro-Jade B, sections after GAD67 immunostaining were washed in three changes of PBS (10 min each), placed on silane-coated slide glasses, and rinsed for 1 min in distilled water. The sections were then stained with 0.00001% Fluoro-Jade B in 0.1% acetic acid for 20 min at room temperature, and washed in three changes of distilled water (for 1 min per wash) (Simpson *et al.*, 2001).

To assess GABA levels during KA-induced gamma oscillations, the animals (eight mutants and eight controls) were killed 20 min after KA administration (20 mg/kg, i.p.). Seven mutants were treated with KA 90 min after pretreatment with DTX (0.5 mg/kg, i.p.), and then killed 20 min after KA injection. Twenty-micrometer-thick parasagittal cryostat sections from fresh-frozen brains were mounted on slides, and this was followed by fixation with an ice-cold PBS solution containing 2% paraformaldehyde/2.5% glutaraldehyde for 10 min. GABA was labeled with anti-GABA primary antibody (1 : 1000; Millipore) and Alexa488-conjugated anti-mouse secondary antibody (1 : 200, Molecular Probes), and the intensity of GABA immunoreactivity (IR) in the hippocampus was analysed. To decrease the variability in staining across animals, samples from different animals were immunostained together. To avoid any sampling bias that could affect GABA IR quantification, two different parasagittal sections from around 1.9 μm and 2.3 μm from bregma were selected per mouse. Staining images were acquired and converted to gray scale, and analysed with IMAGEJ software (NIH, Bethesda, MD, USA). The intensity of GABA IR was measured as a mean gray value in the stratum pyramidale in area CA1, in the stratum lucidum in area CA3 and in the corpus callosum per section. The gray values of area CA1 and area CA3 were normalized by the value of the corpus callosum on the same section, and averaged per mouse.

In vivo *multi-tetrode recording from area CA3*

Naive mice were implanted with a microdrive array consisting of seven independently adjustable tetrodes, six of which were targeted to area CA3 (stereotaxic coordinates from bregma: 1.8 mm lateral; 2.0 mm posterior), and one to the corpus callosum to serve as the reference. The mouse microdrive array for the tetrode recording was originally designed by L. D. Sun, and was custom-made (Accelerated Technologies, Inc., Austin, TX, USA), with some modifications. It was directly connected to an EIB-27-Micro (Neuralynx, Bozeman, MT, USA), and unit recording was conducted using 32 channels of a Cheetah-64 recording system (Neuralynx). After 10 days of recovery from the implantation surgery, the tetrodes were slowly lowered into area CA3 as the mice were sitting quietly in a small, high-walled enclosure (sleep box). Recordings began when stable units were obtained. Recording sessions generally consisted of one or two 'run' epochs (20–30 min each) bracketed by 'sleep' sessions, in which the animal rested quietly on a small platform outside of the behavioral environment. Run sessions were conducted in a low-walled L-shaped linear track (length, 77 cm; width, 7 cm) placed near the center of a square, black-curtained room (10 × 10 ft). Diffuse room lighting was provided by low-intensity spotlights focused on four salient visual cues located on each of the walls of the recording room. Extracellular action potentials during an animal's run were recorded while the animal's position was tracked using a pair of infrared diodes placed 2 cm above its head. All of the data acquired during recording sessions were analysed offline. In order to analyse individual cells in X-CLUST, a manual clustering program (Wilson & McNaughton, 1993), Neuralynx timestamp tracking files and Neuralynx video tracking files were converted to the files on a linux template with the use of a custom interactive program running on a PC workstation. Action potentials were assigned to individual cells on the basis of a spike's relative amplitude across the four recording wires of a tetrode (Nakazawa *et al.*, 2002). In order to be included for analysis, isolated cells had to satisfy three criteria: (i) fire a minimum of 100 spikes during the run session; (ii) have a mean firing rate greater than 0.1 Hz; and (iii) have less than 0.5% of the cell spikes fall within a 1-ms refractory period. All isolated cells were divided into two subclasses – pyramidal cells and interneurons – on the basis of waveform and firing characteristics. Putative pyramidal cells were defined as cells with relatively broad waveforms (peak-to-trough width > 300 ms) and a strong tendency to produce complex spike bursts (complex spike index; CSI > 3%), whereas putative interneurons had relatively narrow waveforms (peak-to-trough width < 240 ms) and few, if any, complex spike bursts (CSI < 3%).

To determine the effect of CA3-NR1 disruption on the firing of CA3 cells, several electrophysiological properties of hippocampal activity were measured. First, two measures were used to assess the output property of individual CA3 cells: mean firing rate and peak firing rate. Second, the bursting tendencies of hippocampal pyramidal cells were measured using two parameters: burst duration and burst spike frequency (the ratio of number of spikes involved in a burst relative to the total number of spikes produced by a cell). Third, spike width (peak-to-trough width) was measured as a measure of the intrinsic properties of pyramidal cells.

Local field potential (LFP) recording from CA1

Five fNR1 mice, three CA3-Cre mice and 10 mutant mice were employed for LFP recording, during which animals received i.p. injections of 20 mg/kg KA. For mutants receiving KA after DTX pretreatment ($n = 9$), LFP recording was conducted as follows: 30 min of recording of background activity, followed by 90 min of recording after DTX pretreatment (0.5 mg/kg, i.p.), followed by over 90 min of recording after KA treatment. Because DTX-induced subconvulsive behavioral seizures were observed about 60 min after treatment, as previously described (Silveira *et al.*, 1988), the last 30-min period before KA treatment was analysed.

The microwire array consists of eight Formvar-insulated nichrome wires (50 μm in diameter; #762000 AM system, Carlsborg, WA, USA), which were aligned in a single slanted row to vary the depth of recording (1-mm span), with an inter-electrode separation of 100 μm. Each microwire was connected with silver paint to the pin of an eight-pin subminiature headpiece connector (Mill-Max Mfg. Corp., Oyster Bay, NY, USA) and securely covered with polyester shrink tubing. One pin was bent to attach an enamel-coated copper ground wire (255 μm in diameter) to the skull during surgery. All of the connection points were finally sealed and stabilized with a thin layer of dental acrylic. The impedance of each electrode wire tip was between 0.2 and

0.5 M? The microwire array was surgically implanted on the skull in the right hemisphere (stereotaxic coordinates from bregma: 1.7 mm lateral; 2.0 mm posterior; 1.4 mm below the cortical surface at maximum depth) to locate the electrode tips from the corpus callosum to the stratum pyramidale or radiatum of area CA1, and fixed with a ground/reference wire to the skull with cranial screws and dental acrylic. Electrode placement in all animals was confirmed after all of the recording procedures were completed, using the histological examination procedures described below. The mice were allowed to recover from anesthesia before being returned to their home cages, and were monitored daily for wellbeing.

After 10 days of recovery from surgery, the microwire array of electrodes was connected to an EIB-27-Micro via a custom-made adaptor, and LFP signals were filtered (bandwidth from 0.1 to 475 Hz), digitized, and acquired at a sampling rate of 1.56 kHz per channel, using eight channels of a Cheetah-64 recording system (Neuralynx Inc.). Animals were intraperitoneally injected with KA at 20 mg/kg, and LFPs were recorded in a rectangular open arena (24 × 18 cm) for 30 min before and for at least 90 min after KA injection. LFP activity monitoring was continued for at least 60 min at 1 day (Day 2) and 7 days (Day 8) after injection. For mutants receiving DTX pretreatment, LFP recording was conducted as follows: 30 min of recording of background activity, followed by 90 min of recording after DTX pretreatment (0.5 mg/kg, i.p.), followed by over 90 min of recording after KA treatment. On Days 2 and 8, LFPs were recorded in the same arena used on the day of injection. Because no significant difference was observed in LFP activity between fNR1 and G32-4-Cre mice, the data from both genotypes were combined as a control. On Day 11, the recording sites were microlesioned by current injection to verify the location of the recording electrodes, and mice were perfused with 4% formalin for Nissl staining.

KA-induced epileptic activity was obtained from the electrodes placed in CA1 cell layer and analysed with NEUROEXPLORER 4 software (Nex Technologies, Littleton, MA, USA). Epileptic discharge in LFP recording was defined by high-frequency and high-voltage synchronous spike activity and/or multi-spike complexes. Epileptiform activity was defined as a brief event of 'spike and wave' discharge or 'burst-like' discharge with no continuous ictal activity. The duration of epileptiform activity was measured from the onset of initial rise to the point where LFP activity trace returned to baseline with no after-discharge period. LFP activity during an entire recording period was also evaluated with spectrograms in NEUROEXPLORER 4. To estimate the KA-induced low-frequency (30–50 Hz) gamma band oscillations, the power spectrum density was analysed using fast Fourier transformation within 2 min before onset of the first epileptic discharge. To calculate the peak power amplitude of gamma band oscillation per animal, we first calculated baseline values of the power spectrum density for each frequency, which was defined as on a linear line between values at the frequencies of 30 and 50 Hz. Peak power amplitude was then measured by subtracting the baseline value from its peak power value. Data from each animal were analysed using STATISTICA 7.0 software (StatSoft Inc., Tulsa, OK, USA).

Off-line analyses of sharp waves (SPWs), ripples, and theta activity

The LFP signals were analysed offline with NEUROEXPLORER 4 software to visually explore raw signals and calculate spectrograms. The electrode located at the corpus callosum served as a reference electrode. Custom-made software written in the LABVIEW program (Vernier Software & Technology, Beaverton, OR, USA) was used to detect and analyse SPWs, ripples, and theta activity. Epochs containing theta activity and SPW–ripples (SPW-Rs) were independently analysed after automatic segmentation of the raw signals in > 15-s epochs. Theta activity was defined by calculating the theta/delta power amplitude ratio as previously described (Csicsvari *et al.*, 1999). Briefly, Fourier components of the theta (5–10 Hz) and delta (2–4 Hz) frequency bands were calculated in 5-s windows using a Hamming window. Theta activity epochs were analysed in segments with a theta/delta ratio > 6. Mean amplitude and peak frequency of the theta band were calculated across all epochs per animal. Theta/delta ratios < 3 epochs were classified as non-theta periods or SPW-R-associated periods, and subjected to ripple and SPW detection algorithms. Ripple events were extracted as previously described (Buzsáki *et al.*, 2003). The raw signals were digitally filtered (80–250 Hz, using a Hamming window-based finite impulse response (FIR) bandpass digital filter), and background mean and standard deviation (SD) were calculated from the power (root mean square) filtered signals. Epochs > 7 SD from the background mean were classified as a ripple; peak-to-trough amplitude was individually measured and averaged for over 100 ripples per animal. In the same time epochs, SPWs were detected in the unfiltered signals by applying a > 4 SD background mean exceeding the threshold. Mean-to-trough amplitude was measured for > 100 SPWs and averaged per animal. Histograms of SPW peak amplitudes were constructed per animal, and averaged for analysis of SPW event distribution across genotypes. In a bimodal event distribution of the mutants obtained, the lower peak corresponded to a 'conventional' SPW, and a peak exceeding 1.8 mV amplitude was defined as a 'giant SPW'. In addition, mean-to-trough amplitude and occurrence were separately analysed for 'conventional' and 'giant' SPWs.

Statistical analysis

Data are presented as means and standard errors of the mean. *N*-values are stated in the figure legends. The statistical significance of electrophysiological data between means of experimental and control groups was determined using Student's *t*-test. Fisher's exact test and Kruskal–Wallis tests were performed to assess the differences in seizure susceptibility between genotypes. Statistical analysis of immunohistochemical data was performed by Kruskal–Wallis test followed by the *post hoc* Mann–Whitney test with Bonferroni's correction for gray value analysis of GABA IR. Analysis of variance (ANOVA) followed by *post hoc* Bonferroni test or Tukey test was used for all other analyses unless otherwise noted. A P-value < 0.05 indicates statistical significance.

Results

Reduced firing and impaired spatial representation in mutant CA3 pyramidal cells with hypersynchronous SPW-R activity

A previous study from our laboratory showed that the place cell activity of CA1 pyramidal cells in a familiar environment in mutant mice was apparently normal (Nakazawa *et al.*, 2002). To assess the basic firing and place cell properties of CA3 pyramidal cells in mutant mice, we used an *in vivo* multi-tetrode recording technique in freely moving mice. Multiple single units from hippocampal area CA3 were recorded as animals ran back and forth on a familiar linear track; 24 pyramidal cells from four mutants and 20 pyramidal cells from three fNR1 controls were quantitatively analysed. There were dramatic decreases in the mean and peak firing rates of mutant CA3 pyramidal cells as compared with those of fNR1 mice (Table 1). The bursting activities of mutant CA3 pyramidal cells, as measured by the duration of a single burst and burst spike frequency (the percentage of spikes

TABLE 1. Properties of CA3 pyramidal cells in familiar linear tracks

Measurement	Floxed-NR1	Mutant
Mean firing rate (Hz)	2.38 ± 0.36	0.55 ± 0.09**
Peak firing rate (Hz)	14.5 ± 2.09	7.46 ± 1.31*
Spike width (μs)	542.8 ± 19.4	574.6 ± 20.2
Burst duration (ms)	10.6 ± 0.3	8.9 ± 0.5*
Burst spike frequency (%)	41.9 ± 2.2	33.4 ± 2.5*

Twenty neurons from three floxed-NR1 controls and 25 neurons from four mutants. Student's *t*-test, *$P < 0.05$, **$P < 0.0005$.

that occurred within bursts), also decreased. No difference was observed in peak-to-trough spike width between the genotypes. In addition, we observed defective CA3 place cell activity during animals' exploration in a familiar open arena (Fig. 1), which could be attributed to impaired firing of the mutant CA3 pyramidal cells.

Hypersynchronous SPW-R activity in mutant area CA1 during immobility

SPW-R complexes originate in area CA3 and propagate to downstream targets, including area CA1 (Chrobak & Buzsáki, 1994, 1996; Csicsvari *et al.*, 2000; Maier *et al.*, 2003; Both *et al.*, 2008). To evaluate the effects of CA3-NR1 ablation on CA1 network oscillations, we assessed LFP activity recorded from area CA1 using seven fNR1 control mice and eight mutant mice in a familiar small open arena for 30 min. We first defined theta and irregular slow activity periods by calculating the ratio of the Fourier components of the theta (5–10 Hz)

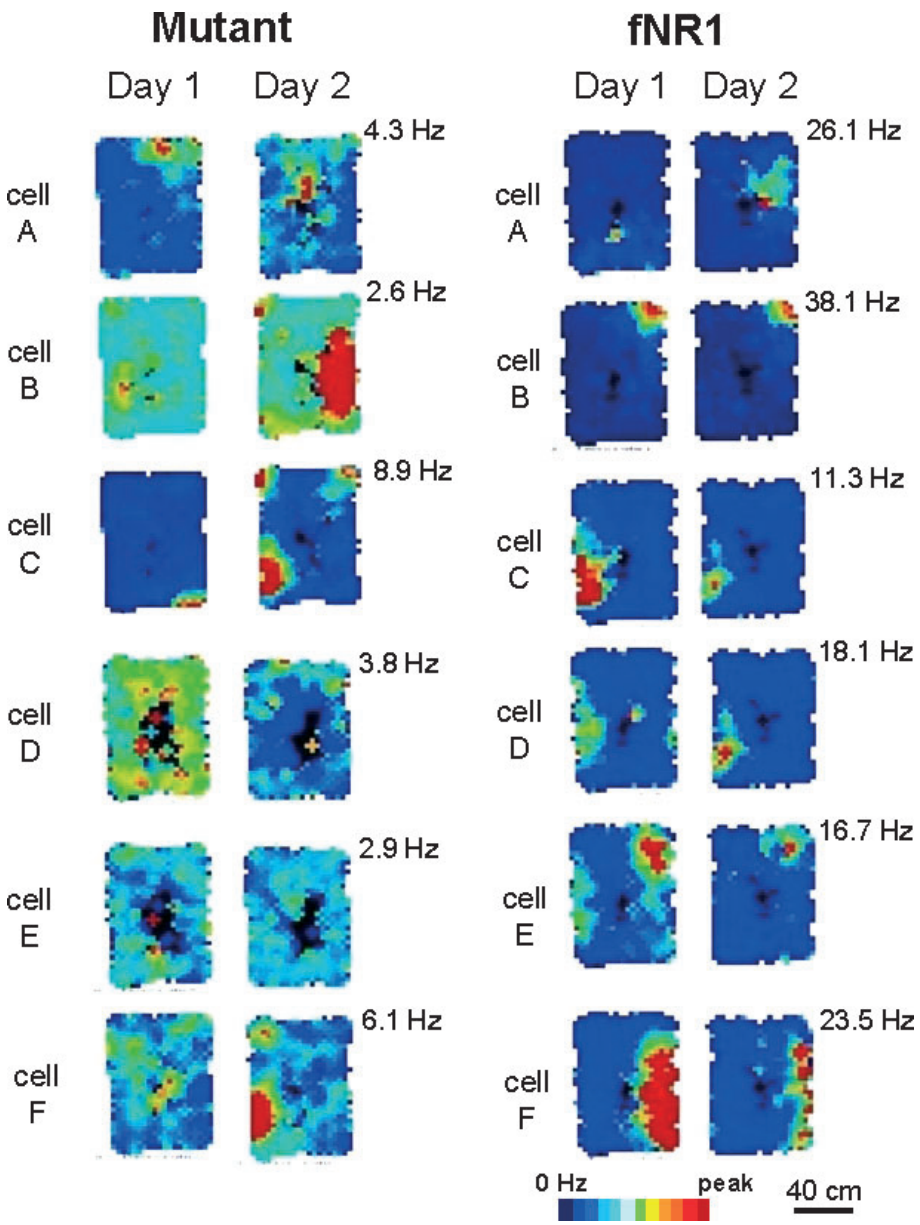

FIG. 1. Mutants are impaired in CA3 place cell activity in a novel and familiar arena. Representative place fields from the same CA3 complex spiking cells (cells A to F) recorded in a novel (Day 1) and familiar (Day 2) rectangular low-walled arena (90 × 60 cm). Firing-rate maps are scaled to the same maximum firing rate per cell across days, as indicated at the upper right corner of the maps. Analysis was restricted to periods when animals were running at > 2 cm/s, and the firing rate was calculated for pixels visited > 10 times. The mutant mice displayed defective CA3 place cell activity, whereas CA3 cells in floxed-NR1 control mice formed stable and spatially confined place fields.

and delta (2–4 Hz) frequency bands (Csicsvari *et al.*, 1999). A ratio of > 6 SD identified theta periods, and epochs with a theta/delta ratio < 3 identified SPW-associated irregular slow activity periods (Hirase *et al.*, 2001). In LFP recordings from the CA1 stratum radiatum, where the SPW activity is most robust in mice (Buzsáki *et al.*, 2003) (Fig. 2B), the magnitude of mutant SPW activity was overall much higher than that of fNR1 mice during SPW-associated periods (Fig. 2A). Strikingly, the mutant SPW peak amplitudes were invariably bimodally distributed (Fig. 2C), and the larger synchronous population activities exceeding 1.8 mV in amplitude, namely 'giant SPW', constituted about 12.7± 2.0% of total SPW events. In contrast, almost no giant SPW activity was observed in the fNR1 control mice in any of the recording periods. The average amplitude of mutant SPWs, excluding 'giant SPWs', was also higher than that in fNR1 controls, regardless of the duration of awake immobilization periods (Fig. 2D; amplitude, 1.04 ± 0.05 mV for mutants and 0.78 ± 0.07 mV for fNR1 mice,

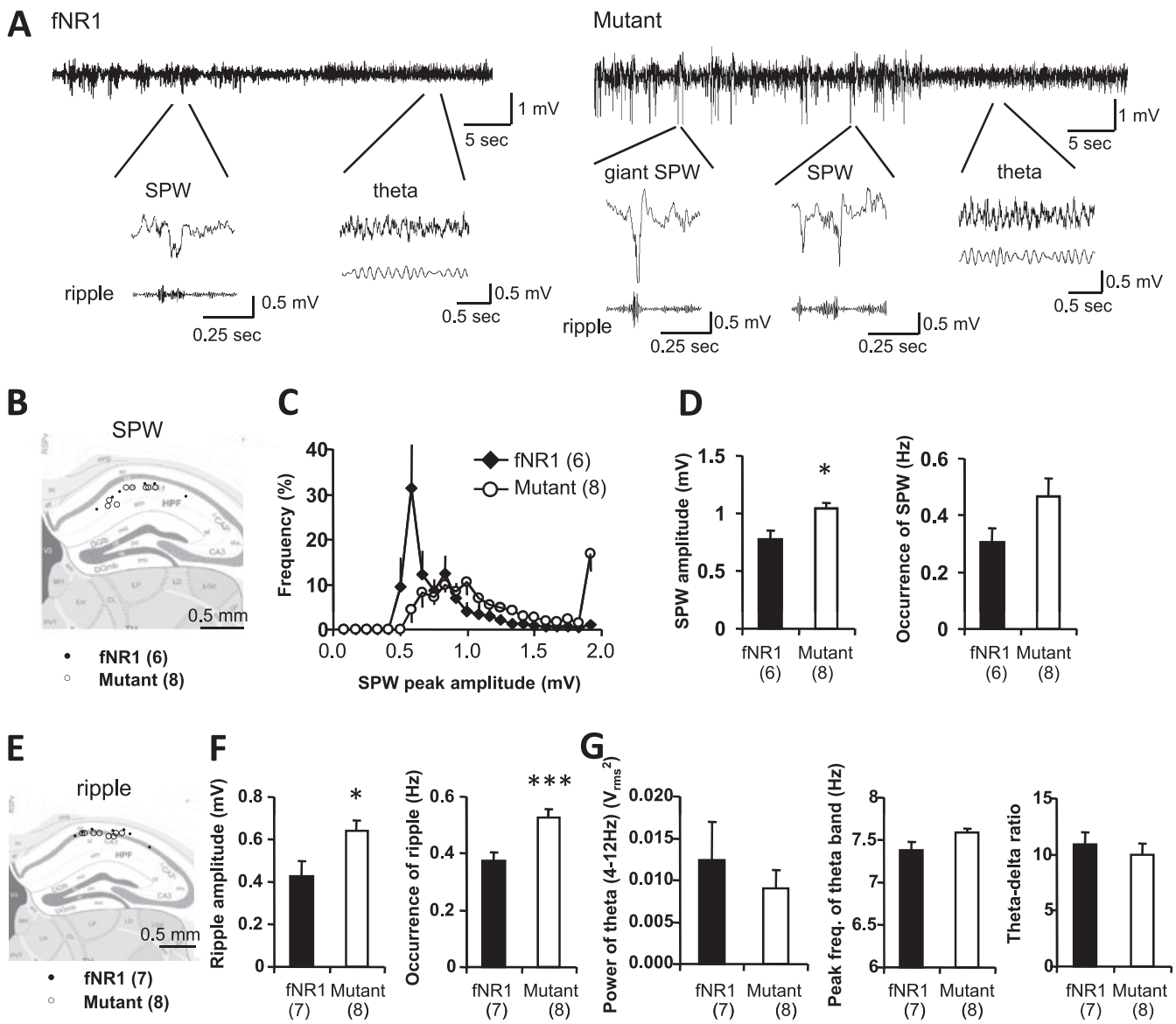

FIG. 2. Augmented sharp wave–ripple (SPW-R) activity and normal theta wave activity in area CA1 of the mutants. (A) Representative local field potential (LFP) traces including theta and SPW-associated periods in floxed-NR1 (fNR1) (left) and mutant (right) mice recorded from the CA1 stratum radiatum. Typical traces of theta waves, 'conventional' SPWs and 'giant SPWs' are magnified below. LFP signals were filtered at 80–250 Hz to detect ripples, and at 5–12 Hz to detect theta waves. (B) Location of individual electrodes implanted in the CA1 stratum radiatum for SPW analysis. (C) Distribution of the peak amplitude of SPWs in fNR1 control (black rhomboids) and mutant (white circles) mice. Strikingly, mutants showed a clear bimodal distribution of SPW peak amplitude. Events with peak amplitude exceeding 1.8 mV were defined as 'giant SPWs', which appeared only in mutants. (D) The amplitude (left) and the occurrence (right) of conventional SPWs in fNR1 and mutant mice during SPW-associated periods. Mutants displayed higher amplitudes (Student's *t*-test, $*P < 0.05$) and an increased tendency to have 'conventional' SPWs (Student's *t*-test, $P = 0.09$). (E) Location of individual electrodes implanted in the CA1 stratum pyramidale for ripple analysis. (F) The amplitude (left) and the occurrence (right) of ripples in fNR1 and mutant mice during SPW-associated periods. Ripple amplitude and occurrence in mutant mice were higher than in fNR1 controls. Student's *t*-test, $***P < 0.005$, $*P < 0.05$. (G) Power (left) and peak frequency (middle) of theta oscillations and theta/delta ratio (right) are shown. Theta/delta ratio was defined as power in the theta peak frequency range (5–10 Hz) divided by power in the delta peak frequency range (2–4 Hz). No significant differences in theta properties were observed between fNR1 and mutant mice, suggesting normal theta activity in mutants. Black bars, control mice; white bars, mutant mice. Numbers in parentheses indicate the numbers of animals.

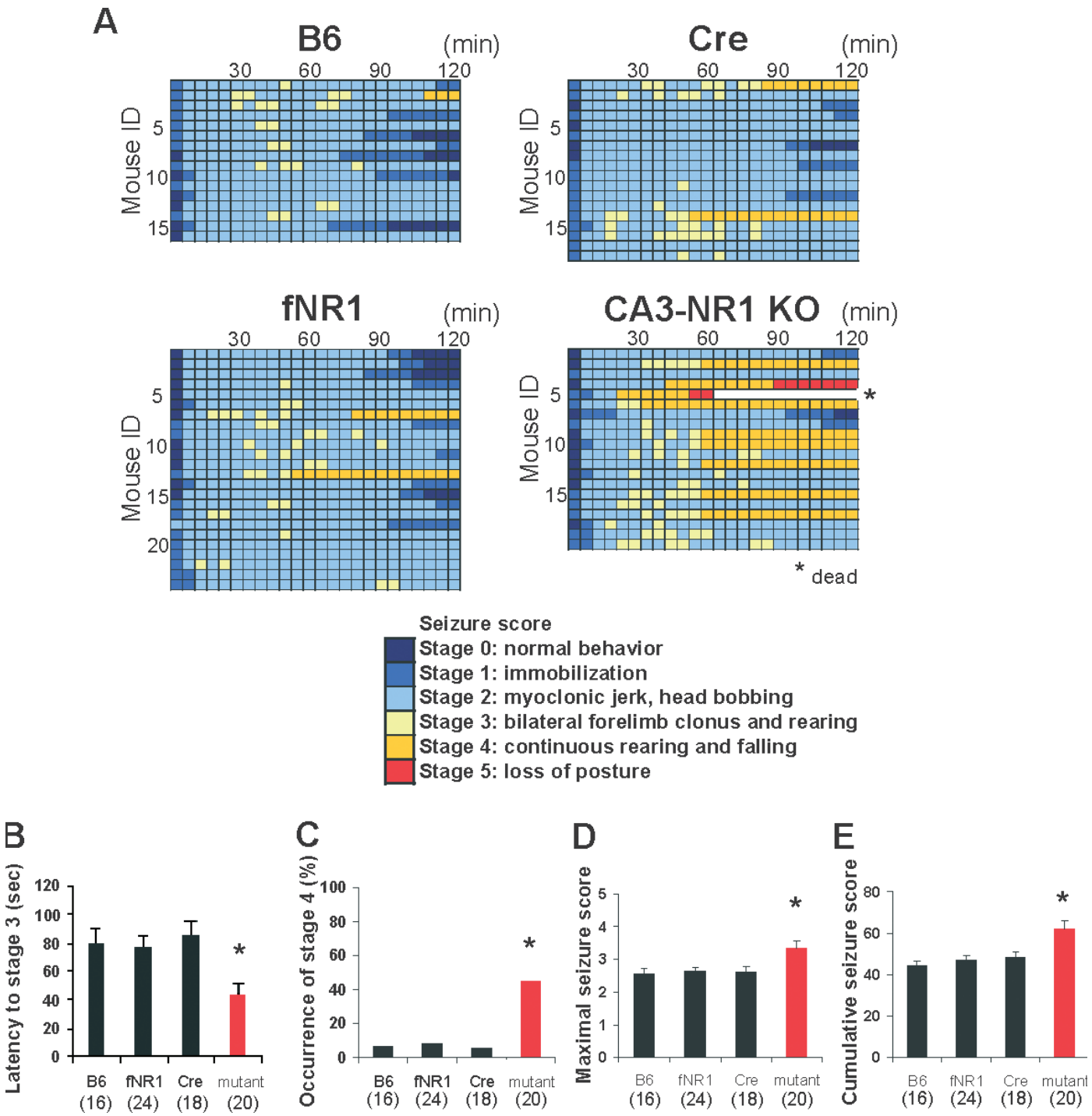

FIG. 3. CA3-NR1 knockout (KO) mice show higher susceptibility to kainic acid (KA)-induced seizures. (A) Time course of seizure severity in each animal of the mutant and three control genotypes [C57BL/6 (B6), floxed-NR1 (fNR1) and Cre] following KA treatment (20 mg/kg, intraperitoneal). The maximum seizure score of each animal was measured every 5 min over a 2-h period. The time scale in one box was 5 min. (B) The latency to stage 3 seizures – forelimb clonus and rearing – was shorter in mutants than in other genotypes. Note that, if the animal did not show stage 3 seizures, the latency was considered to be as 120 min (Kruskal–Wallis test, $*P < 0.05$). (C) The occurrence of stage 4 seizures – continuous rearing and falling – was higher in mutants than in other genotypes (Fisher's exact test, $*P < 0.05$). (D and E) Mutant mice showed a higher severity of seizure than any of the control genotypes. Columns represent the averaged maximum seizure score (D) and cumulative seizure score (E) measured over a 2-h period after KA injection (Kruskal–Wallis test, $*P < 0.05$). Black bars, fNR1 mice; red bars, mutant mice. The numbers in parentheses indicate the numbers of animals.

Student's *t*-test, $P < 0.05$). Furthermore, the occurrence of SPWs showed a tendency to increase (0.47 ± 0.07 Hz for mutants and 0.31 ± 0.05 Hz for fNR1 mice, Student's *t*-test, $P = 0.09$). Similarly, the averaged amplitude and the occurrence of fast oscillatory ripple activity recorded from CA1 pyramidal cell layer in the mutants were both higher than those of fNR1 controls (Fig. 2E and F; amplitude, 0.64 ± 0.05 mV for mutants and 0.43 ± 0.07 mV for fNR1 mice, Student's *t*-test, $P < 0.05$; occurrence, 0.53 ± 0.03 Hz for mutants and

0.37 ± 0.03 Hz for fNR1 mice, Student's *t*-test, $P < 0.005$). These results suggest that NR1 ablation in CA3 pyramidal cells elicits a state of hypersynchrony in the CA3 recurrent network, which propagates to area CA1, thus generating larger and more frequent SPW-R events. It is also plausible that the reduced firing of mutant CA1 GABAergic cells (Nakazawa *et al.*, 2002) contributes to the augmented SPW-R activity in area CA1.

The oscillatory activity during the theta periods in the mutants was normal overall. No differences were observed in the power, peak frequency or occurrence of theta bands between the genotypes (Fig. 2G). Importantly, no 'giant SPW' events or paroxysmal activities were detected during the theta period, which was consistent with the evidence in the mutants showing normal CA1 place cell activity and spatial learning in the familiar environment (Nakazawa *et al.*, 2002, 2003) as well as no behavioral seizures induced by audiogenic or tactile stimuli (data not shown). These results suggest that the mutant mice were, overall, not epileptic.

Mutants were more susceptible to KA-induced seizures

Because KA targets limbic structures and induces epileptic discharges (Ben-Ari *et al.*, 1981), we used it to test the long-standing hypothesis that hypersynchronous discharges reflected in CA3 SPWs play a causal role in the generation of limbic epilepsy (Prince, 1978; Traub & Wong, 1982; Buzsáki, 1986). We first determined that an i.p. injection dose of 20 mg/kg animal body weight of KA induced minimal continuous rearing and falling (stage 4 seizures) and hippocampal damage in fNR1 control mice of a B6 background (supporting Fig. S1). Mice of four genotypes received i.p. KA injections – the mutant mouse strain and three control groups: B6 wild-type, fNR1, and G32-4-Cre. Behavioral seizures were evaluated for at least 2 h, using a modified Racine's score (Fig. 3). We found that the latency to stage 3 seizures was significantly shorter in mutants than in controls, and stage 4 seizures, maximum seizure score, and the cumulative number of seizures were all more frequent in the mutants than in the control genotypes. Two of the 14 mutants experienced stage 5 seizures, and one of them died after the treatment, whereas none of the three control genotypes progressed to stage 5 seizures or died. These results suggest that the mutant mice exhibit an increased susceptibility to KA-induced seizures.

CA1 selective neurodegeneration in mutant hippocampus was induced by KA

Whereas the inbred C57BL/6 strain is resistant to neurodegeneration (Schauwecker & Steward, 1997; McKhann *et al.*, 2003; McLin & Steward, 2006), increased seizure severity induced by KA treatment may result in increased excitotoxicity in the mutant brain. To evaluate the extent of excitotoxicity induced by KA at the dose of 20 mg/kg, Nissl staining was conducted on parasagittal sections of mutants (Fig. 4A and B) and fNR1 controls (supporting Fig. S2, A and B) that manifested stage 4 or more severe seizures during the first 2-h period after treatment. In the hippocampus of mutants 1 day after KA injection, we observed extensive excitotoxic alterations, as revealed by highly condensed pyknotic nuclei in the CA1 cell layer, but not in area CA2/CA3 or the DG (Fig. 4B). Four weeks after KA injection, extensive cell loss was prominent in the CA1 pyramidal cell layer of mutants, whereas no apparent degeneration was observed in the CA2/CA3 cell layer or DG granule cell layer. In contrast, almost no hippocampal cell loss was detected in the fNR1 mice in any subfield at any stage following KA administration (supporting Fig. S2, B). Because the results in B6 wild-type and G32-4-Cre mice were almost identical to those observed in fNR1 mice, we used the results from fNR1 mice to represent the control genotype in all subsequent histological analyses.

To detect KA-induced neurodegeneration with higher sensitivity, fNR1 and mutant mice underwent KA i.p. treatment, and brain sections were processed for NeuroSilver staining. Consistent with Nissl staining, most CA1 pyramidal cells were silver-stained from 1 day to 1 week after KA treatment in all the mutants that manifested stage 4 or more severe seizures (graph in Fig. 4C, $F_{3,32} = 27.62$ for genotype × time interaction in area CA1, $P < 0.00001$, untreated mutant vs. mutant at 1 day and 7 days after KA treatment, $P < 0.0005$; fNR1 vs. mutant at 1 day and 7 days after KA treatment, $P < 0.0005$). In contrast, almost no silver-impregnated cells were observed in area CA2/3, the DG, the subiculum, the entorhinal cortex, or the lateral septum (supporting Fig. S2, C–F), suggesting that these brain areas are unlikely to be KA-induced epileptic loci in the mutants. These stained cells largely disappeared within 4 weeks after treatment, probably owing to immunological clearance of dead cells. In contrast, in control fNR1 mice, almost no staining was found in any brain area, despite the fact that some mice had shown equivalent stages of KA-induced seizure. To confirm the KA-induced neurodegeneration, sections from both genotypes were stained with Fluoro-Jade B, a high-affinity fluorescent marker for the localization of neuronal degeneration (Schmued & Hopkins, 2000). In the mutant hippocampus, the distribution of Fluoro-Jade B-stained cells largely coincided with that of the silver-impregnated cells, confirming that neurodegeneration was localized to area CA1 in the mutant hippocampus (Fig. 4E).

To further investigate this issue, we examined whether seizure severity correlated with KA-induced excitotoxic cell damage in the hippocampus. We used Nissl staining for morphological analyses of fNR1 mice ($n = 30$) and mutant mice ($n = 29$) 1–4 weeks after KA treatment, including the mice depicted in Figs 3 and 4A–C. Figure 4D shows three-dimensional histogram plots of the maximum seizure score for the first 2 h after KA treatment, as compared with subsequent damage in the CA1 cell layer for each genotype. Mutants showed a clear correlation between the severity of seizure and the extent of CA1 cell damage, but the two scores were not correlated in fNR1 controls (Pearson coefficient for mutants, $r = 0.74$, $P < 0.00005$; Pearson coefficient for fNR1 mice, $r = 0.27$, $P = 0.14$; genotype effect, $P < 0.05$). Furthermore, the mutant damage scores were bimodally distributed, and about 40% of mutants with less severe seizure scores exhibited no CA1 degeneration. In contrast, most fNR1 mice (28 of 30) showed CA1 cell death regardless of the severity of seizure scores.

KA-induced epileptic discharges with attenuated gamma oscillation in area CA1 of mutants

To explore the underlying mechanisms by which CA3-NR1 ablation resulted in KA-induced excitotoxic cell death in area CA1, we assessed LFP activity in area CA1. LFP recordings were performed during the first 90 min, 1 and 7 days after KA injection, using electrodes implanted into the dorsal area CA1 in fNR1 mice ($n = 5$), Cre control mice ($n = 3$), and mutant mice ($n = 10$). All of the KA-treated animals carrying a microwire array exhibited typical behavioral seizures, similar to those described in Fig. 5A, lasting for several hours and subsiding spontaneously on that day. Because the results from fNR1 and Cre mice were almost identical, these results were combined and treated as a 'control' genotype. During the acute phase, highly synchronous epileptic discharges repeatedly occurred in area CA1 of both control (trace 1) and mutant (traces 3 and 5) mice (Fig. 5A). The latency to epileptic discharges after KA injection was significantly shorter in mutants than in control mice (Fig. 5B). The occurrence of epileptic discharge events during the first 90 min after

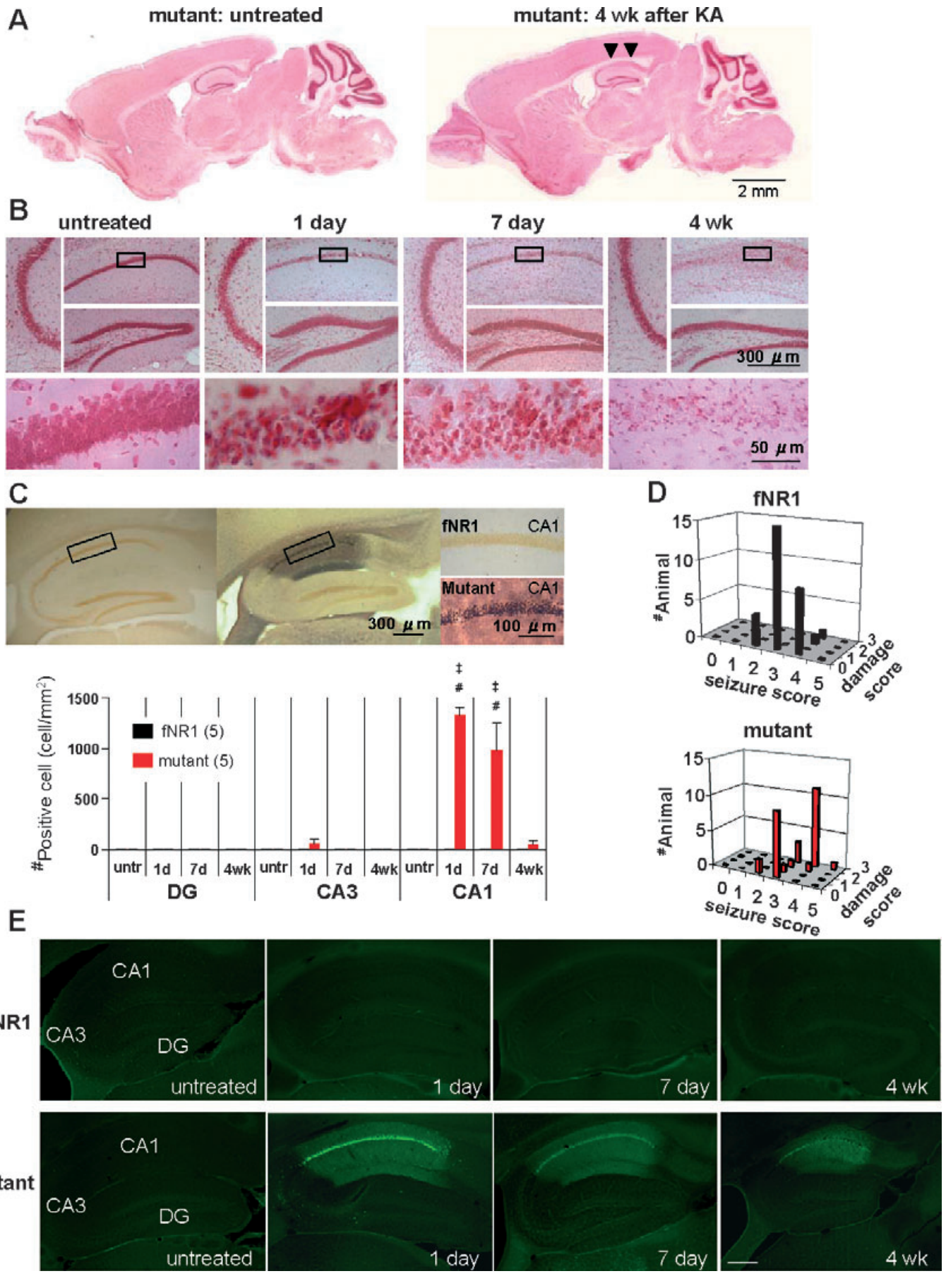

KA treatment was also higher in mutants (Fig. 5C). Cumulative epileptic discharge duration during this period was also longer in mutants than in controls (Fig. 5D). It is conceivable that the magnitude of mutant epileptic discharges could contribute to CA1 neurodegeneration. In fact, when mutants were subdivided into two groups according to the CA1 damage score shown in the middle panel of Fig. 9A, the magnitude of epileptic discharge events was much more robust in the mutants that eventually showed cell death in area CA1 (group B) than in those that did not (group A) (Fig. 5C and D).

In control mice, another prominent KA-induced oscillatory activity was low-frequency (30–50 Hz) gamma band oscillation, which appeared approximately 15–20 min after KA injection and 10 min before the onset of the first epileptic discharge (trace 2 in Fig. 5A and E). This is consistent with reports of KA-induced 30–40-Hz oscillatory synchronous activity in the rodent hippocampus *in vivo* (Medvedev *et al.*, 2000; Khazipov & Holmes, 2003; Sakatani *et al.*, 2008). However, the LFP power spectrogram of mutant area CA1 (Fig. 5F) revealed a significantly lower magnitude of 30–50-Hz gamma band oscillations during this period in the mutants than in the controls (trace 6 in Fig. 5A and E). Remarkably, KA-induced gamma band oscillatory activity almost disappeared in group B mutants (those with cell death); in contrast, this activity remained observable in group A mutants (those without cell death; Fig. 5G). Because group A mutants exhibited gamma oscillations despite a short latency to epileptic discharges (Fig. 5B), this effect in group B mutants did not appear to be due to gamma oscillations being obscured by epileptic discharges. These results suggest that the magnitude of 30–50-Hz gamma oscillations before onset of epileptic discharges was inversely correlated with the degree of CA1 excitotoxicity.

Epileptiform activity was sustained in mutant area CA1

To further explore the process leading to CA1 neurodegeneration in the mutants, LFP recording was continued on the day following KA injection. LFP activity in area CA1 of fNR1 or Cre control mice showed no continuous ictal discharges and was almost indistinguishable from that observed before KA treatment. However, area CA1 in the mutants exhibited epileptiform activity characteristic of large-amplitude spike-like discharges on Day 2 (Fig. 6A), although they displayed no continuous ictal discharges. Among mutants, group A (non-cell death) mutant mice displayed 'spike and wave' discharges superimposed on normal background activity. In contrast, group B mutant mice, having undergone massive CA1 degeneration, showed polyspike discharges with longer durations on top of the suppressed background activity. Quantitative analysis revealed that the occurrence of such epileptiform activity, which was rarely observed in the controls, was higher in group B than in group A mutants (Fig. 6B). The duration of individual epileptiform activity was also longer in group B mutants (Fig. 6C). Remarkably, polyspike discharge-type epileptiform activity was still present in group B mutants at least 7 days after KA treatment, whereas simple 'spike and wave' discharges were rarely observed in group A mutants (Fig. 6D). These results suggest that the massive CA1 neurodegeneration observed in group B mutants resulted from the polyspike discharge-type epileptiform activity observed on day 2.

KA-induced degeneration of mutant area CA1 GABAergic cells

Attenuation of low-frequency gamma oscillations in the acute phase and the subsequent epileptiform activity on the following days in the group B mutants could reflect a deficit in CA1 GABAergic network activity upon KA administration. To evaluate the integrity of hippocampal GABAergic networks, we quantified the NeuroSilver-positive cells in the mutant CA1 subfield in the NeuroSilver-stained sections shown in Fig. 4C. Prominent increases in NeuroSilver-positive cells were observed not only in the cell layer (stratum pyramidale) but also in other strata 1 day after KA treatment (Fig. 7A), suggesting neurodegeneration of CA1 interneurons. Fluoro-Jade B-positive sections (Fig. 4E) were also immunostained with antibody against GAD67, the GABA-synthesizing enzyme, and double-labeling confirmed degeneration of mutant GABAergic interneurons in area CA1 (Fig. 7B).

To further examine the extent of the damage to the degenerated interneurons, we quantified the GAD67-positive cells in untreated and KA-treated animals that showed stage 4 or more severe seizures (Fig. 7C). The number of GAD67-positive cells in area CA1 of fNR1 control mice decreased 1 day after KA treatment, but returned to the levels seen in untreated mice within 1 week (Fig. 7D). In contrast, the number of GAD67-positive cells in the CA1 subfield of the mutants decreased to less than 50% of that in fNR1 control mice 1 day after injection, and was unchanged 4 weeks after treatment. In the mutants, regional analysis revealed a severe and permanent KA-induced reduction of GAD67-positive cells in all strata as compared with fNR1 mice, except for cells in the stratum lacunosum–moleculare (Fig. 7E). Notably, the total numbers of GAD67-positive cells in the stratum oriens ($\sim$150 cells/mm^2) and stratum radiatum ($\sim$50 cells/mm^2) (see 'untreated' cell number in Fig. 7E) were similar to the numbers of mutant NeuroSilver-positive cells in the same strata 1 day after KA treatment (Fig. 7A), suggesting that, although most GABAergic neurons in the mutants transiently suffered neurodegeneration upon KA administration, at least 60% of GABAergic cells in these CA1 strata showed permanent loss of GAD67 IR, presumably coinciding with cell death. On the other hand, the number of mutant NeuroSilver-positive cells in the stratum lacunosum–moleculare ($\sim$50 cells/mm^2) was far lower than the total number of GAD67-positive cells in the same strata ($\sim$200 cells/mm^2). Their

FIG. 4. Kainic acid (KA)-treated mutant mice showed massive neurodegeneration in area CA1. (A) Nissl-stained parasagittal brain sections of mutant untreated mice (left) and mutant mice 4 weeks after KA treatment (right). KA-treated mutants showed severe neuronal loss in area CA1 (indicated by arrowheads). (B) Magnified hippocampal subfields, CA1, CA3, and dentate gyrus (DG), in untreated mutant mice, or mutant mice 1 day, 7 days and 4 weeks after KA injection. Each bottom panel shows a higher magnification of the boxed area in the mutant area CA1. Note that highly condensed pyknotic nuclei, a typical sign of damaged nuclei, were observed in the mutant CA1 pyramidal cell layer from 1 day to 7 days after KA injection, eventually disappearing by 4 weeks post-treatment. (C) NeuroSilver staining showed massive neuronal degeneration in mutant area CA1 7 days after KA treatment. NeuroSilver-positive cells were not detected in the floxed-NR1 (fNR1) control hippocampus. The graph on the right shows the number of NeuroSilver-positive cells in the hippocampal subfields of both genotypes. The number of NeuroSilver-positive cells in the mutant area CA1 was significantly higher than in controls at 1 day or 7 days post-injection (Tukey's *post hoc* test: untreated mutant vs. mutant at 1 day and 7 days after KA treatment, $^{\ddagger}P < 0.0005$; fNR1 vs. mutant at 1 day and 7 days after KA treatment, $^{\#}P < 0.0005$). Black bar, fNR1 mice; red bar, mutant mice. The numbers in parentheses indicate the number of animals for each time point. (D) Three-dimensional plots of maximum seizure scores (*x*-axis) vs. damage scores (*y*-axis) of fNR1 (left) and mutant (right) mice 1 to 4 weeks after KA treatment. The *z*-axis shows the number of animals. Neuronal damage was evaluated according to the damage score scale (see Materials and methods). Black bars, fNR1 mice; red bars, mutant mice. (E) Fluoro-Jade B staining revealed massive neuronal degeneration, predominantly in area CA1 of the mutant mice, 1 day, 7 days and 4 weeks after KA treatment, whereas almost no staining was observed in fNR1 controls and in untreated mouse sections, regardless of genotype.

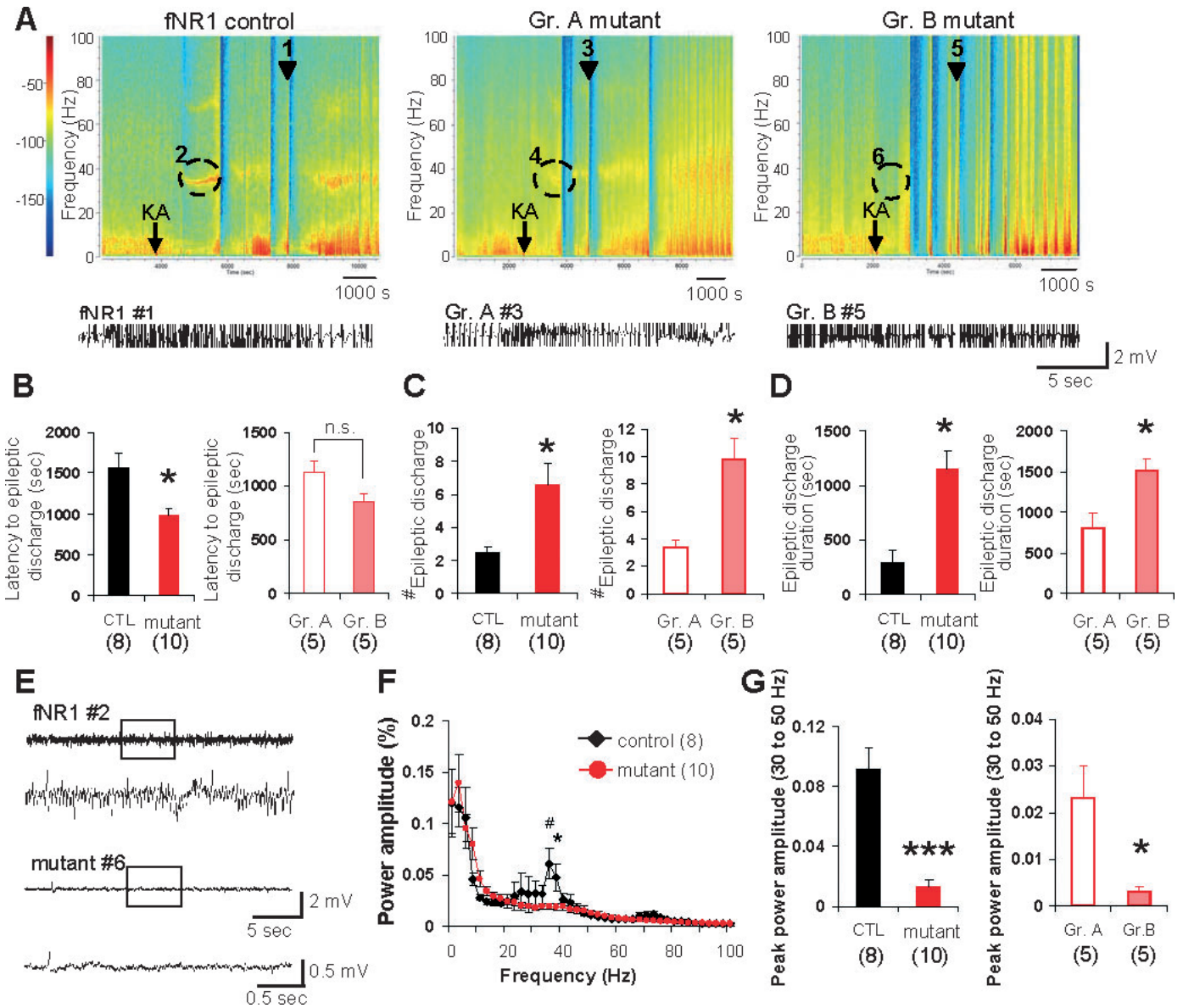

FIG. 5. Increased epileptic discharges with diminished gamma oscillation upon kainic acid (KA) injection. (A) Representative spectrograms of KA-induced local field potential (LFP) activity from floxed-NR1 (fNR1) controls (left) and mutants (middle and right). Mutants were subdivided into two groups: group A (middle), which did not show cell death, and group B (right), in which CA1 cell death was eventually observed, on the basis of the CA1 damage score shown in the middle panel of Fig. 9A. Arrows indicate the timing of KA intraperitoneal injection. Color: log of power spectral densities. Epileptic discharge traces of a representative fNR1 mouse (marked as #1 in the spectrogram) and group A and group B mutant mice (marked as #3 and #5, respectively) are also shown below each spectrogram. (B) Left: the latency to epileptic discharges after KA treatment was shorter in mutant mice (n = 10) than in controls (CTL) (n = 8; five fNR1 mice and three Cre mice). Right: group A 'non-cell death' mutants (n = 5) and group B 'cell death' mutants (n = 5), as defined above (Student's t-test, $^{*}P < 0.05$). No difference in latency to epileptic discharge was noted between the two mutant groups (Student's t-test). n.s., not significant. (C) Left: epileptic discharges during the 90 min after KA treatment occurred in mutant mice (n = 10) more frequently than in controls (n = 8; five fNR1 mice and three Cre mice). Right: the number of discharges was higher in group B mutants than in group A mutants (Student's t-test, $^{*}P < 0.05$). (D) Left: the average duration of individual epileptic discharge events was longer in mutants than in controls. Right: among mutants, group B mutants showed longer epileptic discharge duration than group A mutants (Student's t-test, $^{*}P < 0.05$). (E) Representative traces of 30–50-Hz gamma band oscillatory activity, which preceded the first epileptic discharge, in fNR1 mice (upper trace) and group B mutant mice (bottom trace) mice (marked as #2 and #6, respectively in Fig. 5A). Boxed periods in each upper trace are magnified in the bottom traces. (F) LFP power spectra in area CA1. The power amplitude of the 30–50-Hz gamma band during the 2 min before the onset of the first epileptic discharge was significantly diminished in mutants (red-filled circles) as compared with controls (filled rhomboids) (Student's t-test, $^{\#}P < 0.01$ for 35 Hz, $^{*}P < 0.05$ for 37.5 Hz). (G) Left: the peak power amplitude of 30–50-Hz gamma band oscillation in mutants was significantly attenuated as compared with controls. Right: this attenuation was more prominent in group B mutants than in group A mutants (Student's t-test, $^{***}P < 0.00005$, $^{*}P < 0.05$). Black bar, fNR1 control mice; red bar, mutant mice; open red bar, group A mutant mice; pink-filled bar, group B mutant mice. The numbers in parentheses indicate the numbers of animals.

GAD67 activity was also largely restored 1 week after KA treatment. Because the main input to stratum lacunosum–moleculare interneurons comes from the entorhinal cortex (Klausberger & Somogyi, 2008) (and not from area CA3), the results suggest that CA1 GABAergic cells receiving reduced output selectively from area CA3 suffered severe neurodegenerative change upon KA treatment.

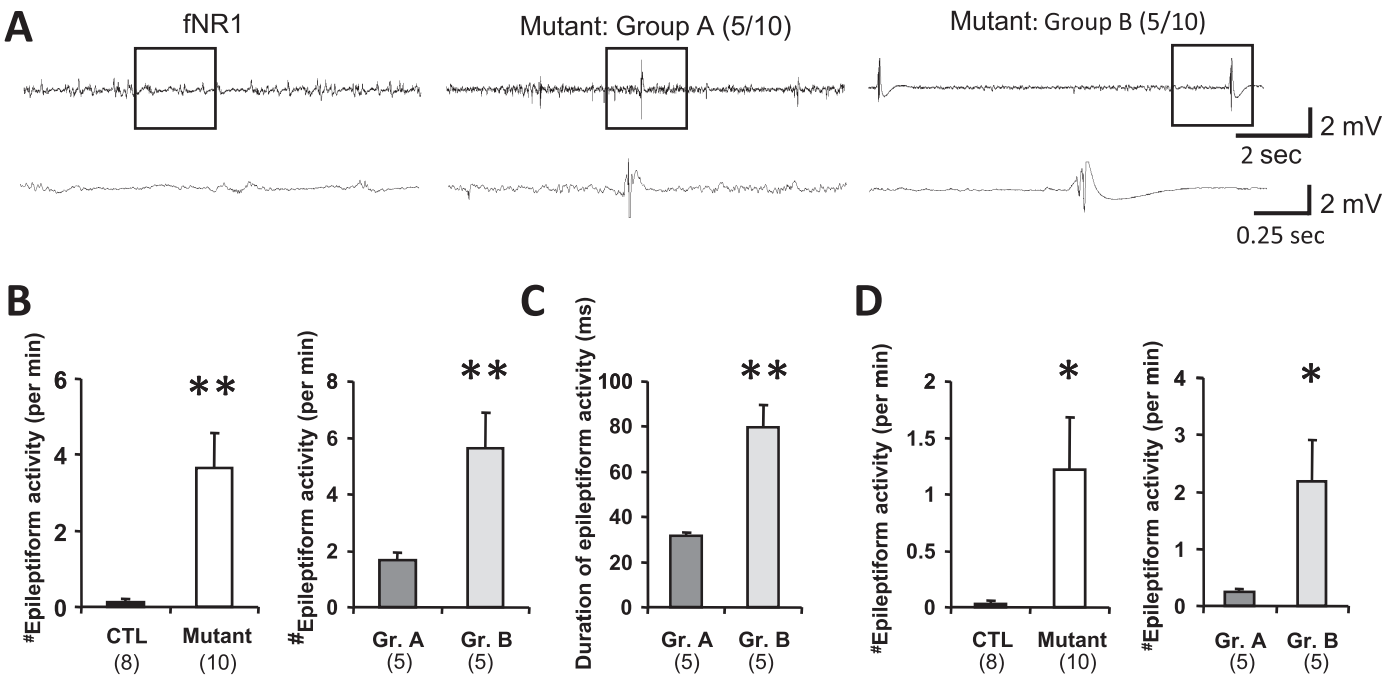

FIG. 6. Sustained epileptiform activity leading to cell death in area CA1 of mutant mice. (A) Representative local field potential activity traces recorded 1 day after kainic acid (KA) treatment in floxed-NR1 (fNR1) controls (left), group A 'non-cell death' mutants (middle), and group B 'cell death' mutants (right). Boxed periods in each upper trace are magnified in the bottom trace. Epileptiform activity was present in mutants 1 day after treatment; controls showed almost normal activity. Group A mutants sporadically showed spike and wave discharges with concomitant background activity, whereas group B mutants displayed a burst suppression-like pattern. (B) Group B mutants showed a higher occurrence of epileptiform activity than group A mutants (right). Almost no activity was observed in control mice (CTL, left) (Mann–Whitney *U*-test, $^{**}P < 0.005$). (C) Group B mutants showed a longer duration of brief epileptiform activity events than group A mutants (Student's *t*-test, $^{**}P < 0.005$). (D) Burst-like epileptiform activities were still detected in group B mutants 7 days after KA treatment (right), but were rarely observed in group A mutants or control mice (left) (Mann–Whitney *U*-test, $^{*}P < 0.05$). Black bar, fNR1 mice; white bar, mutant mice; dark gray bar, group A mutant mice; light gray, group B mutant mice. The numbers in parentheses indicate the numbers of animals.

Pretreatment with DTX restored mutant KA-induced gamma oscillation, GAD67 activity, and resistance to CA1 neurodegeneration

GABAergic interneuron activity suppresses excitotoxicity during seizures (Ylinen *et al.*, 1991; Mody, 1998). Therefore, we wondered whether boosting GABA levels before the onset of the first seizure discharge could protect against CA1 neurodegeneration in the mutants. To test this, we used DTX, a D-type potassium channel blocker, because it acts on presynaptic voltage-gated potassium channels of cortical interneurons (Weller *et al.*, 1985; Richards *et al.*, 2000; Cunningham & Jones, 2001; Shimada *et al.*, 2007) and is a potent enhancer of presynaptic GABA release. The extent to which DTX pretreatment affected presynaptic release was assessed by anti-GABA IR in the CA1 cell layer, where axon terminals of GABAergic interneurons extensively arborize. We first confirmed that there were no obvious effects of a subconvulsive dose of DTX (0.5 mg/kg, i.p.) prior to KA treatment on CA1 SPW-R activity in the mutants (Fig. 8). This was not surprising, because SPW-R activity is generated in area CA3, where GABAergic function seemed to be normal in the mutants (supporting Fig. S3).

We then evaluated several parameters for LFP activity and CA1 excitotoxicity by injecting KA 90 min after DTX pretreatment. Figure 9A shows the histograms of behavioral seizure scores for each animal after KA injection, as well as the CA1 damage score 10 days after the treatment. We found that the behavioral seizure score (Fig. 9B) and the number and duration of mutant epileptic discharges (Fig. 9C) were not affected by DTX pretreatment, which was unexpected. Furthermore, the damage scores in DTX-pretreated mutants were dramatically lower than in saline-pretreated mutants (Fig. 9A and B). Remarkably, DTX pretreatment in mutants also evoked robust low-frequency gamma oscillations before the onset of seizure discharges (Fig. 10A, trace 1 for seizure discharge and trace 2 for gamma oscillation), and the magnitude of gamma oscillations was equivalent to those observed in fNR1 or Cre control mice (Fig. 10B), suggesting that DTX-sensitive, voltage-gated potassium channels are instrumental in synchronizing KA-induced gamma oscillations.

In parallel, KA-induced GABA increases were assessed by comparing GABA IR levels in area CA1 with the IR level of the corpus callosum, where few GABAergic cells are localized (Fig. 10C and D). GABA IR levels in the CA1 cell layer 20 min after KA treatment were significantly higher than in the corpus callosum in controls, which is consistent with previous studies demonstrating KA-induced GABA release in the hippocampus (Zhang *et al.*, 1990; Ding *et al.*, 1998). Remarkably, the CA1 cell layer in mutants showed no increased GABA levels in response to KA injection, but a significant increase was seen after pretreatment with DTX. The deficit in KA-induced GABA increases appeared to be specific to area CA1 in mutants, because no difference was observed in other subfields.

To further evaluate the effects of DTX-induced gamma oscillations on subsequent days, the peak power amplitude of gamma oscillations and the occurrence of epileptiform activity on Day 2 were plotted for all the animals, including the mutants pretreated with DTX (Fig. 10E). We found that the number (Fig. 10E) and duration (Fig. 10F) of epileptiform activities in the pretreated mutants were decreased in comparison with the saline-pretreated mutants. Moreover, the number

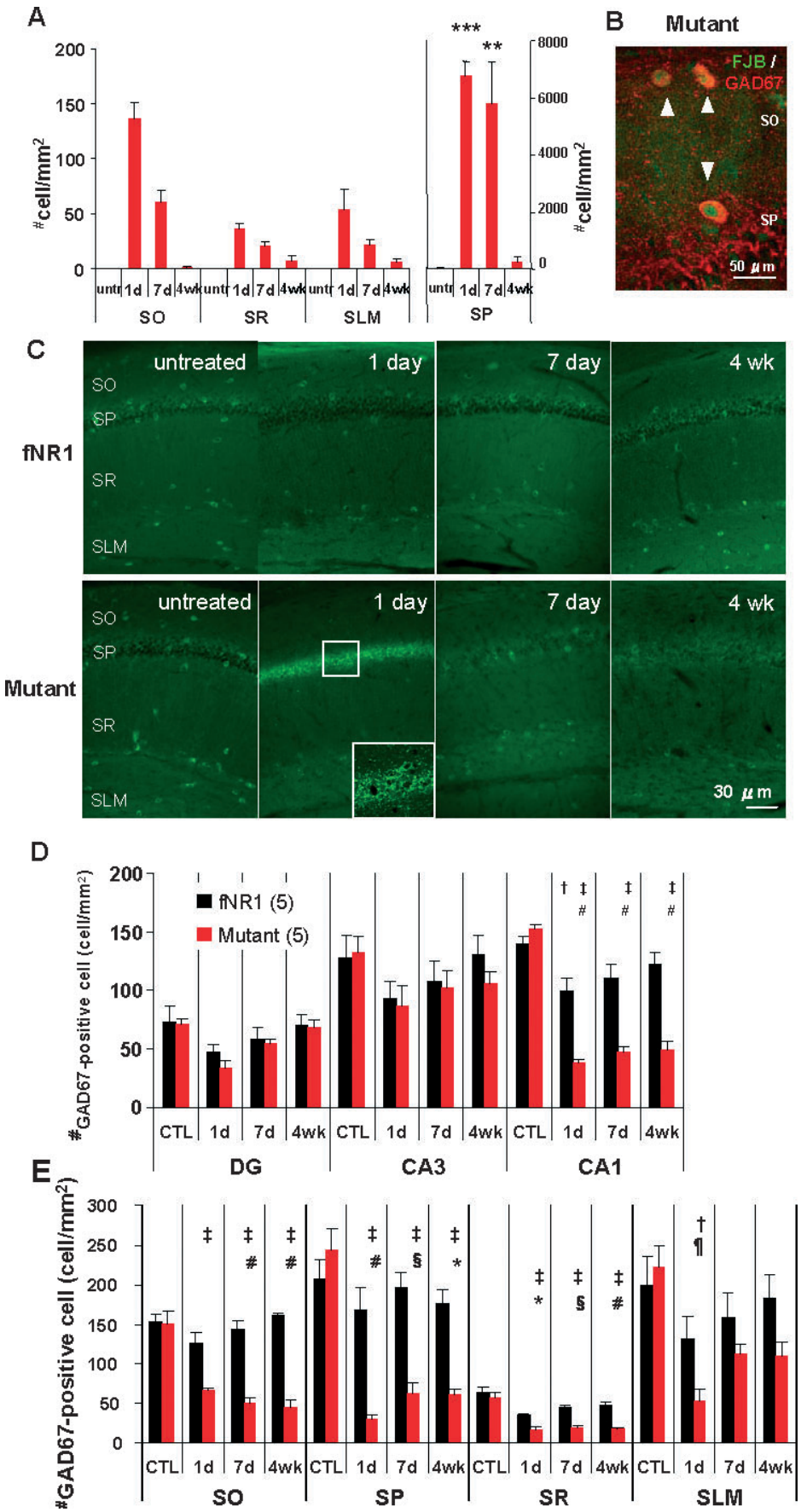

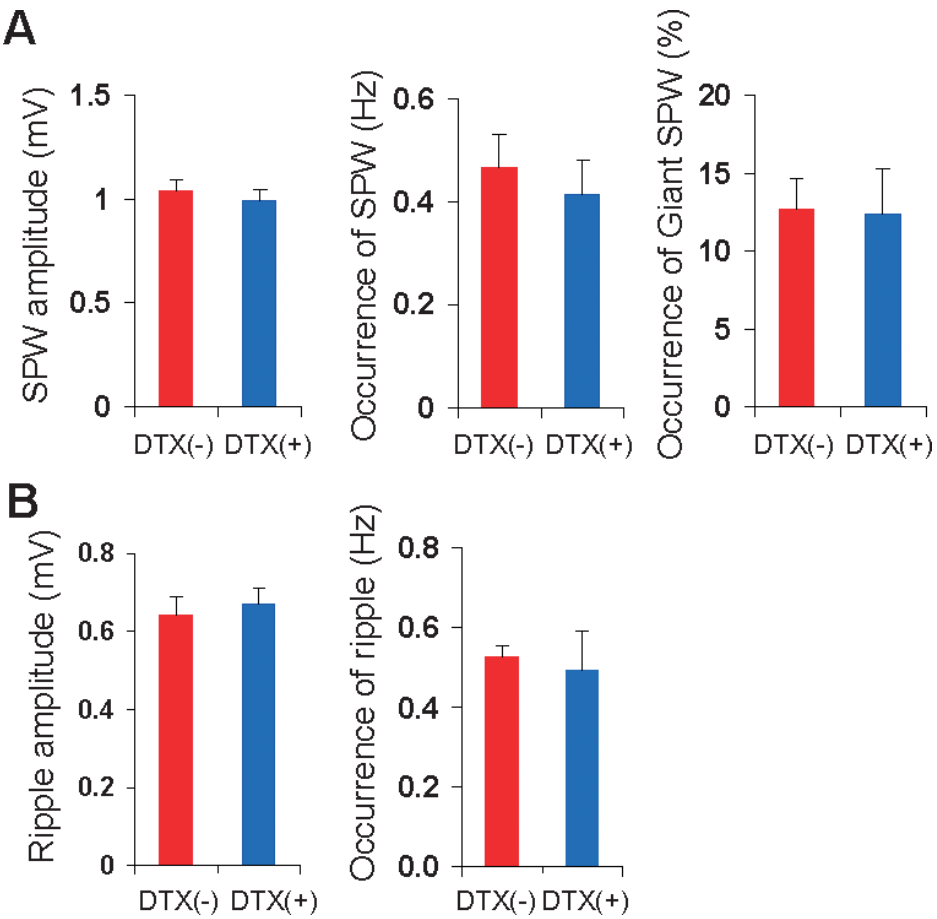

FIG. 8. α-Dendrotoxin (DTX) treatment did not affect mutant sharp wave–ripple (SPW-R) complex activity. (A) The amplitude (left) and occurrence (middle) of conventional SPWs, and the occurrence (relative value) of giant SPWs (right) in mutants before (red) and after (blue) DTX treatment ($n = 9$). (B) The amplitude (left) and the occurrence (right) of mutant ripples before (red) and after (blue) DTX treatment ($n = 9$). No significant change in SPW-R activity was observed before and after DTX treatment (Student's *t*-test, $P = 0.09$, $P = 0.61$, $P = 0.88$, $P = 0.68$ and $P = 0.73$ for SPW amplitude, SPW occurrence, the ratio of giant SPWs, ripple amplitude, and ripple occurrence, respectively). The numbers of animals, $n = 9$.

of CA1 GAD67-positive cells in mutants was also equivalent to that found in fNR1 mice 1 week later (Fig. 10G), suggesting that DTX-induced low-frequency gamma band oscillations restored CA1 GABAergic cell function. Accordingly, 10 days after DTX and KA treatment, almost no CA1 degeneration was observed in the mutants as revealed by NeuroSilver staining (Fig. 9B).

Discussion

The present study had several salient findings: (i) CA3-NR1 KO mutants displayed reduced CA3 pyramidal cell firing, impaired CA3 spatial representation, and augmented SPW-R activity; (ii) systemic KA treatment of the mutants resulted in impaired KA-induced

FIG. 7. Massive neurodegeneration of mutant CA1 interneurons after kainic acid (KA) treatment. (A) Quantification of NeuroSilver-positive cell number in the mutant CA1 subfield in NeuroSilver-stained sections in Fig. 4C. One day after KA treatment, the number of NeuroSilver-positive cells was significantly increased in the entire subfield [$F_{3,16} = 94.2$ for the stratum oriens (SO), $P < 0.00001$; $F_{3,16} = 21.8$ for the stratum pyramidale (SP), $P < 0.0001$; $F_{3,16} = 13.0$ for the stratum radiatum (SR), $P < 0.0005$; $F_{3,16} = 5.84$ for the stratum lacunosum–moleculare (SLM), $P < 0.01$; Tukey's *post hoc* test, untreated mutant vs. mutant at each time point after KA treatment, $^{***}P < 0.0005$, $^{**}P < 0.001$, $^{*}P < 0.05$]. (B) Confocal double staining image of Fluoro-Jade B (FJB, green) with 67-kDa isoform of glutamic acid decarboxylase (GAD67) immunoreactivity (IR) (red) 1 day after KA treatment, showing the degenerating GABAergic neurons in area CA1. (C) Differential changes in GAD67 IR in area CA1 of floxed-NR1 (fNR1) mice and the mutant mice 1 day, 7 days and 4 weeks after KA treatment as compared with their untreated CA1 areas. The inset shows a confocal higher magnification of the boxed area in area CA1, indicating the elevated GAD67 IR, presumably localized to GABAergic neuron axon terminals. In mutant mice, GAD67 IR in the CA1 cell layer was paradoxically augmented 1 day after treatment (inset), suggesting massive GABA release, which was not observed in control mice. (D) Quantification of GAD67-positive cells in the hippocampal subfields for each genotype. The number of GAD67-positive cells in the mutant CA1 areas was significantly lower in the fNR1 area CA1 1 day, 7 days and 4 weeks after KA treatment; no differences were observed in area CA3 or the dentate gyrus (DG) ($F_{3,32} = 12.2$ for genotype × time interaction in area CA1, $P < 0.00005$; Tukey's *post hoc* test, $^{\dagger}P < 0.05$ for untreated fNR1 vs. fNR1 1 day after KA treatment, $^{\ddagger}P < 0.0005$ for untreated mutant vs. mutant at each time point after KA treatment, $^{\#}P < 0.0005$ for fNR1 vs. mutant at each time point). CTL, controls. (E) Quantification of GAD67-positive cells inside the CA1 subfield for each genotype. The number of mutant GAD67-positive cells was severely and permanently decreased in the entire subfield except for the SLM, as compared with the fNR1 control mice ($F_{3,32} = 10.7$ for genotype × time interaction in the SO, $P < 0.00005$; $F_{3,32} = 8.60$ for genotype × time interaction in the SP, $P < 0.0005$; $F_{3,32} = 3.24$ for genotype × time interaction in the SR, $P < 0.05$; $F_{3,32} = 1.56$ for genotype × time interaction in the SLM, $P = 0.21$; Tukey's *post hoc* test, untreated mutant vs. mutant at each time point after KA treatment, $^{\dagger}P < 0.05$, $^{\ddagger}P < 0.0005$, fNR1 vs. mutant at each time point, $^{\P}P < 0.05$, $^{*}P < 0.01$, $^{\S}P < 0.005$, $^{\#}P < 0.0005$). Black bars, fNR1 mice; red bars, mutant mice. The numbers in parentheses indicate the number of animals for each time point.

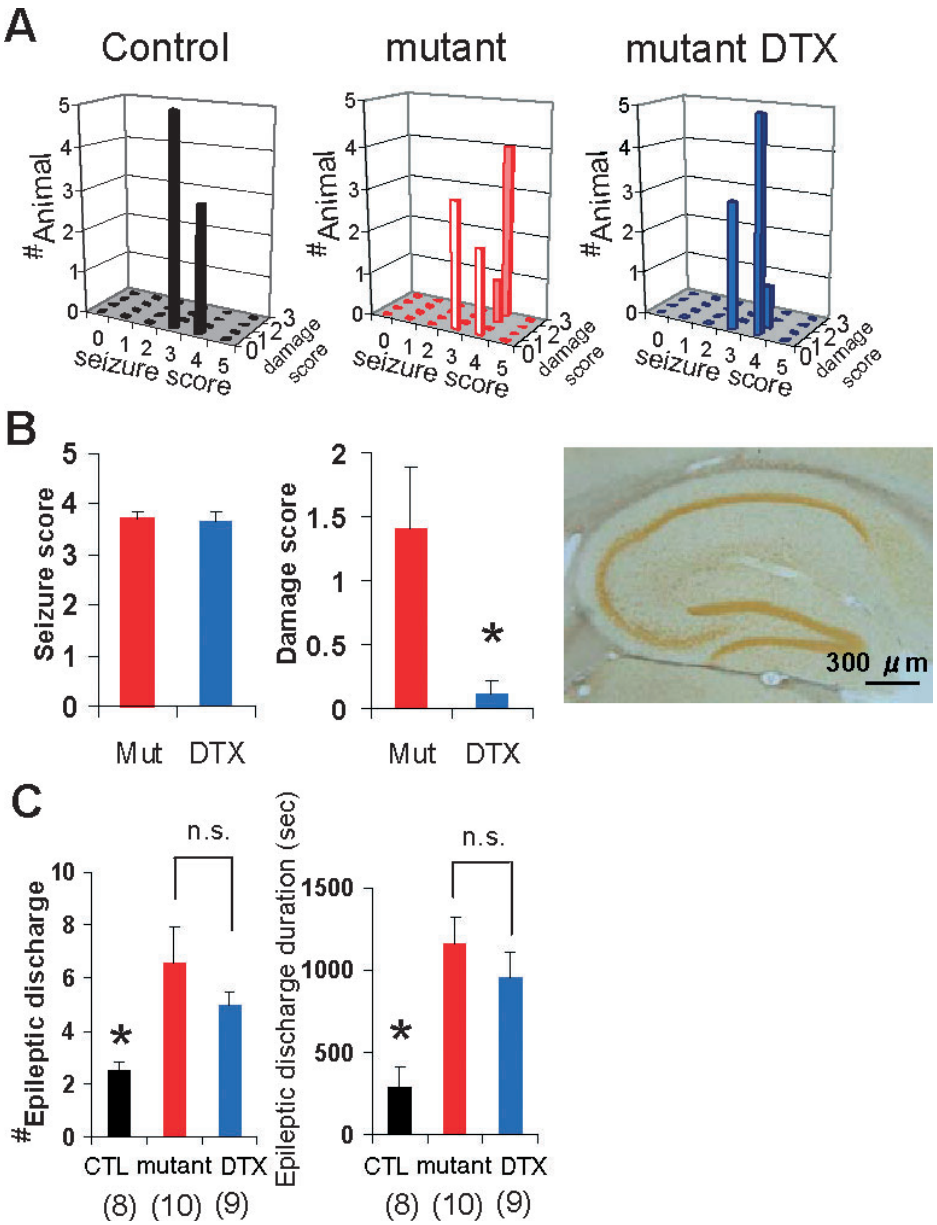

FIG. 9. Pretreatment with α-dendrotoxin (DTX) protected CA1 cells from neurodegeneration but failed to attenuate the severity of epileptic discharges in mutant mice. (A) Three-dimensional plots of the maximum behavioral seizure scores (*x*-axis) vs. the CA1 damage scores (*y*-axis) of floxed-NR1 mice (left, $n = 8$), mutant mice (middle, $n = 10$) and DTX-pretreated mutant mice (right, $n = 9$) during the 90 min after kainic acid (KA) treatment. The *z*-axis shows the numbers of individual mice. A subconvulsive dose (0.5 mg/kg) of DTX protected mutants from massive KA-induced CA1 cell damage. The severity of behavioral seizures induced by KA was not affected by DTX. (B) Quantification of the CA1 damage score (middle) in mutants with or without DTX pretreatment suggests that DTX prevented KA-induced excitotoxicity (Student's *t*-test, $*P < 0.05$). No difference was observed in behavioral seizure scores between the genotypes (left). Right: representative photomicrograph of NeuroSilver staining in area CA1 from DTX-pretreated mutants 1 week after KA treatment, showing no cell death in area CA1. (C) The number (left) and duration (right) of mutant epileptic discharges during the 90 min after KA injection was not affected by DTX pretreatment. DTX-pretreated mutants had a higher number of epileptic discharges, and discharges of longer duration, than control (CTL) mice, but there were no differences for both measures between DTX-pretreated mutants and mutants without DTX pretreatment. (discharge number, Kruskal–Wallis test, $P < 0.005$, Mann–Whitney *U*-test with Bonferroni correction for multiple comparisons, $P < 0.05$ for controls vs. DTX-pretreated mutants, $P = 1.0$ for mutants vs. DTX-pretreated mutants; discharge duration, $F_{2,24} = 8.86$, $P < 0.005$, Bonferroni *post hoc* test, $P < 0.05$ for controls vs. DTX-pretreated mutants, $P = 1.0$ for mutants vs. DTX-treated mutants). The numbers in parentheses indicate the numbers of animals. n.s., not significant.

GABAergic activation and 30–50-Hz gamma oscillations – these were accompanied by augmented seizure discharges, thereby leading to massive and strikingly selective neurodegeneration in area CA1; (iii) in the mutants, the magnitude of KA-induced gamma oscillations was inversely correlated with the magnitude of epileptiform activity, the degree of CA1 degeneration, and the viability of GAD67-positive cells in the days following KA treatment; and (iv) pretreatment with DTX, which restored CA1 GABA levels, maintained mutant KA-induced gamma oscillations and GAD67-positivity, thereby preventing the mutant CA1 cells from excitotoxic cell death. Taken together, the results indicate that a lack of KA-induced gamma oscillations before onset of seizure discharges correlates with prolonged seizure activity and CA1 excitotoxicity, suggesting that persistent gamma oscillations predict resilience to excitotoxic insults.

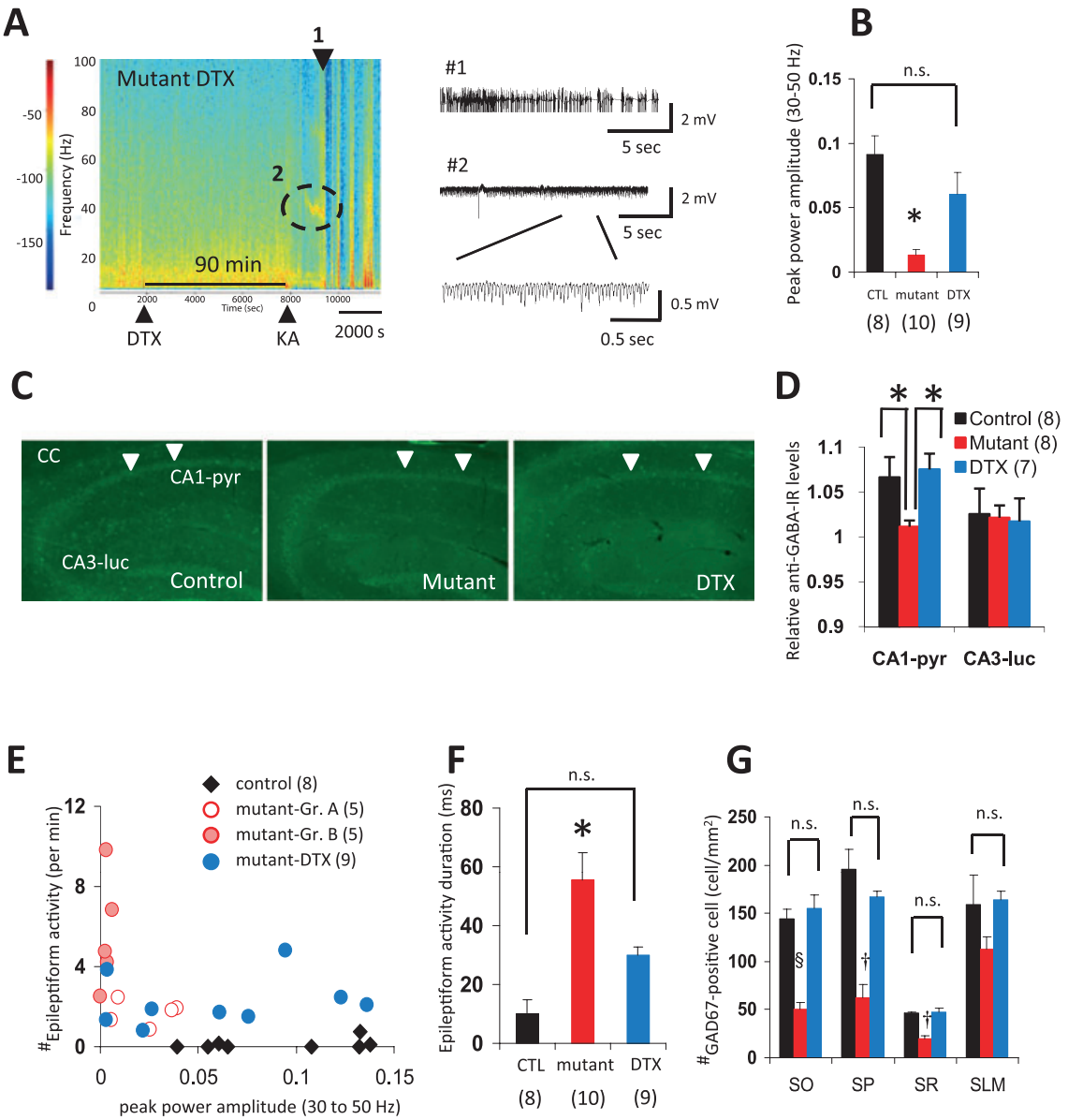

FIG. 10. Pretreatment with α-dendrotoxin (DTX) restored gamma oscillation and the activity of the 67-kDa isoform of glutamic acid decarboxylase (GAD67) and reduced epileptiform activity and CA1 degeneration. (A) Left: a representative spectrogram of kainic acid (KA)-induced local field potential activity in DTX-pretreated mutants. DTX injection was performed 90 min before KA injection. Color: log of power spectral densities. Right: epileptic discharge trace (marked as #1) and a representative trace of 30–50-Hz gamma band oscillatory activity (marked as #2) of DTX-pretreated mutants. (B) Peak power amplitude of 30–50-Hz gamma band oscillations in the DTX-pretreated mutants was significantly higher than in mutants without DTX, and was the same as in control (CTL) mice, suggesting that low-frequency gamma oscillations were restored by DTX pretreatment ($F_{2,24} = 9.98$, $P < 0.001$, Bonferroni *post hoc* test, $P = 0.32$ for controls vs. DTX-pretreated mutants, $^{*}P < 0.05$ for mutants vs. DTX-treated mutants). (C) Representative photomicrographs of γ-aminobutyric acid (GABA) immunoreactivity (IR) of controls (left), mutants (middle) and mutants with DTX pretreatment (right) 20 min after KA treatment. Arrowheads indicate CA1 cell layers. (D) An increase in GABA level was observed in the CA1 pyramidal cell layer (CA1-pyr) but not in the stratum lucidum in area CA3 (CA3-luc) in control animals 20 min after systemic KA intraperitoneal injection. This KA-induced GABA release was abolished in the mutants, but restored after pretreatment with DTX. This mutant deficit was observed in the CA1 cell layer, but not in area CA3. Images were obtained with a confocal microscope and a ×10 objective. The relative GABA IR values were normalized to the level of corpus callosum IR (Kruskal–Wallis test followed by *post hoc* Mann–Whitney test with Bonferroni's correction, $^{*}P < 0.05$). (E) Scatter plot of the peak power amplitude of gamma oscillations vs. the number of events of epileptiform activities 1 day after KA treatment of floxed-NR1 (fNR1) mice (filled rhomboids), mutants (open red circles for group A mutants; pink circles for group B mutants), and DTX-pretreated mice (blue circles). Each dot represents an individual mouse. DTX reduced the epileptiform activity and restored low-frequency gamma oscillations. (F) The duration of the mutant epileptiform activity 1 day after KA treatment was dramatically decreased by DTX pretreatment ($F_{2,24} = 11.7$, $P < 0.0005$ for genotype effect, Bonferroni *post hoc* test, $P = 0.15$ for controls vs. DTX-pretreated mutants, $^{*}P < 0.05$ for mutants vs. DTX-pretreated mutants). (G) Quantitative analysis of GAD67-positive cell in the CA1 subfield 1 week after KA treatment showed no differences between control mice and DTX-pretreated mutants, suggesting that DTX pretreatment fully preserved GABAergic function in the mutant area CA1. Black bars, fNR1 mice; red bars, mutant mice; blue bars, DTX-pretreated mutant mice [$F_{2,13} = 24.21$ for the stratum oriens, $P < 0.00005$, Bonferroni *post hoc* test, $P = 1.0$ for controls vs. DTX-pretreated mutants, $^{§}P < 0.0001$ for mutants vs. DTX-treated mutants; $F_{2,13} = 25.9$ for the stratum pyramidale, $P < 0.00005$, Bonferroni *post hoc* test, $P = 0.44$ for controls vs. DTX-pretreated mutants, $^{†}P < 0.0005$, for mutants vs. DTX-trreated mutants; $F_{2,13} = 20.6$ for the stratum radiation, $^{†}P < 0.0001$, Bonferroni *post hoc* test, $P = 1.0$ for controls vs. DTX-pretreated mutants, $^{†}P < 0.0005$ for mutants vs. DTX-treated mutants; $F_{2,13} = 2.17$ for the stratum lacunosum-moleculare, $P = 0.15$, Bonferroni *post hoc* test, $P = 1.0$ for controls vs. DTX-pretreated mutants]. $^{*}P < 0.05$, $^{§}P < 0.0001$, $^{†}P < 0.0005$, n.s., not significant.

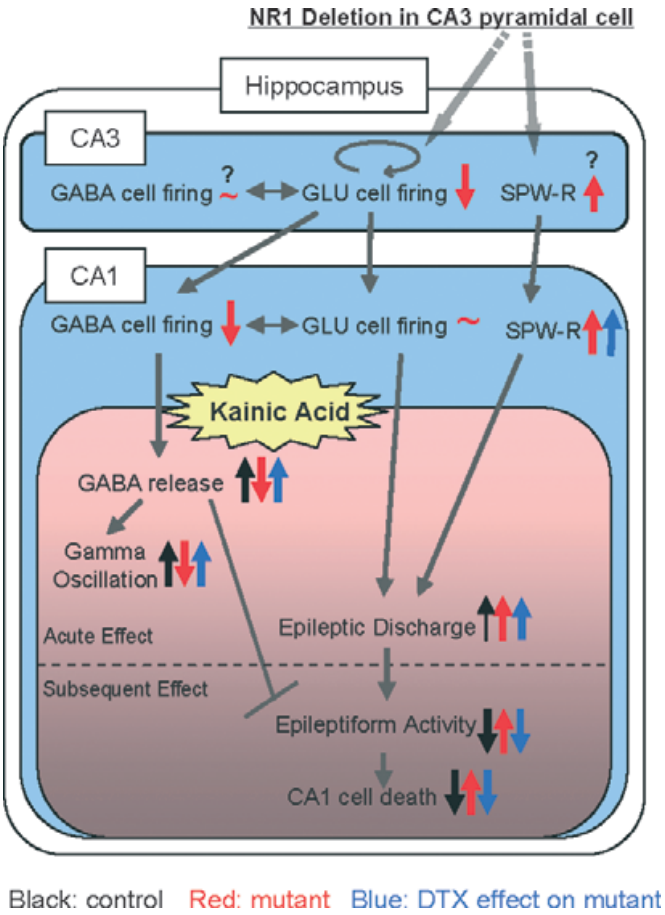

FIG. 11. Kainic acid (KA)-induced gamma oscillations and CA1 cell death in CA3-NR1 knockout mice. Depiction of how the CA3–CA1 network activity (blue) is affected by genetic deletion of CA3–NR1, and, upon KA administration, there is selective neurodegeneration of CA1 (pink). Postadolescent NR1 elimination in CA3 pyramidal cells (GLU cells) diminishes their action potential firing, thereby reducing the firing of CA1 interneurons [γ-aminobutyric acid (GABA) cell], while CA1 pyramidal cell activity is maintained by reduced feedforward inhibition. Simultaneously, CA3-NR1 deletion abnormally enhances sharp wave–ripple (SPW-R) activity in area CA3. An intermediate dose of KA (20 mg/kg, intraperitoneal) facilitates GABA release, thereby eliciting 30–50-Hz gamma oscillations within 20 min, and then evoking epileptic discharge-burst activity in the control animals (black arrow). However, this dose does not extend the epileptic discharges to sustained epileptiform activity on the following days, and consequently, no cell death is observed in the control hippocampus. In contrast, KA-induced GABA release and gamma oscillations do not occur in area CA1 of the mutants, presumably because of reduced excitability of CA1 interneurons, and epileptic discharges are instead exacerbated, and SPW-R activity is enhanced (red arrow). A presynaptic GABA release enhancer, DTX (blue arrow), has no effect on mutant SPW-R activity and seizure severity after KA administration. Remarkably, however, it assists in KA-induced GABA release, which maintains the integrity of the CA1 GABAergic network, thereby preserving gamma oscillations, suppressing epileptiform activity, and further protecting mutant area CA1 from KA-induced excitotoxicity. These results suggest that KA-induced GABA release may prevent epileptic discharges from transforming the sustained epileptiform activity and causing a deterioration in GAD67-positive cells, resulting in no neurodegeneration of CA1 neurons. Overall, the emergence of KA-induced gamma oscillations correlates with a good prognosis following KA-induced hippocampal excitotoxicity in mice. The question mark denotes putative action/change.

Increased susceptibility to KA-induced seizure and CA1 excitotoxicity following CA3-NR1 ablation

To explore the relationship between gamma oscillations and excitotoxicity, it was essential to employ CA3-NR1 KO mice (referred to as 'mutants' throughout this article). In these mice, two possibly interrelated events were observed following genetic NR1 ablation of CA3 pyramidal cells during adulthood (Nakazawa *et al.*, 2002) – a dramatic decrease in CA3 pyramidal cell firing/bursting, and augmented SPW-R activity. It is not obvious how functional ablation of CA3-NRs could decrease action potential generation. In fact, the firing rates of CA1 pyramidal cells lacking the same NR1 subunit were almost the same as those of control mice (McHugh *et al.*, 1996). The results obtained here could be due to the mutual reduction of afferent drive from nearby CA3 pyramidal cells as well as the inhibition of cell firing by CA3 interneurons (Freund & Buzsáki, 1996). Another possibility, which is not mutually exclusive, is that CA3-NRs could contribute to normal excitatory synaptic transmission, as described in the adult visual cortex (Miller *et al.*, 1989), the sensory thalamus (Kemp & Sillito, 1982; Salt, 1986), and the red nucleus (Davies *et al.*, 1986), or could even contribute to action potential generation (Zhao *et al.*, 2005).

On the other hand, increased SPW-R activity during immobility is paradoxical, given that CA3 recurrent network activity is low, because generation of CA3 SPW-Rs apparently requires CA3 recurrent network activity (Csicsvari *et al.*, 2000; Behrens *et al.*, 2005). Whereas NR antagonists prevent the induction of the SPW-R complex (Behrens *et al.*, 2005), NRs seem to be unnecessary for maintaining spontaneous SPW-Rs once the SPW-Rs are established (Behrens *et al.*, 2005) or in the ventral portions of hippocampal area CA3, where spontaneous SPW-Rs are observed (Papatheodoropoulos & Kostopoulos, 2002; Maier *et al.*, 2003; Colgin *et al.*, 2004). Rather, the magnitude of CA3 SPW-Rs nearly doubled following the application of an NR antagonist in rat slices, perhaps via mechanisms that involve decreased Ca^{2+} influx through NRs and subsequent inactivation of SK type 2 Ca^{2+}-activated potassium channels mediating afterhyperpolarization (Colgin *et al.*, 2004). Because CA3-NR1 was eliminated along the longitudinal axis, including the ventral area CA3, in the mutants (Nakazawa *et al.*, 2002), spontaneous SPW-Rs could become larger in the ventral area CA3 after postadolescent NR1 ablation, subsequently spreading to the dorsal area CA3 and further to area CA1. Although the mechanisms underlying the generation of spontaneous 'giant SPWs' are unknown, impaired Ca^{2+}-activated afterhyperpolarization could play a role, because its abnormal regulation may contribute to epileptiform discharges (Fernández de Sevilla *et al.*, 2006). Alternatively, 'giant SPWs' could be a consequence of decreased CA3 pyramidal cell firing, because spontaneous oscillatory bursting seems to be a common characteristic of tetrodotoxin-treated neurons (Ramakers *et al.*, 1990; Trasande & Ramirez, 2007).

Consequently, in this study, the mutants displayed increased susceptibility to KA-induced seizures and CA1 excitotoxicity, owing to impaired GABAergic function in area CA1 of the hippocampus, and abnormally high SPW-R activity during periods of immobility. One plausible explanation for the remarkably selective CA1 neurodegeneration seen here is that reduced afferent drive from CA3 to CA1 interneurons in a feedforward manner leads to a coherent loss of postsynaptic inhibition in area CA1 upon KA treatment, thus rendering CA1 cells vulnerable to excitotoxicity. Interestingly, almost no CA3 cell death in mutants was observed, despite reduced afferent drive from the recurrent network.

The KA dose used here for systemic injection (20 mg/kg, i.p.) was instrumental in determining the cellular process by which KA injection led to neurodegeneration of mutant CA1 cells. Approximately half of the mutants manifested massive and irreversible cell loss in the CA1 cell layer; in contrast, the other half displayed almost no cell death (Figs 4D and 9A). This non-cell death group (group A mutants) became an excellent animal control in the same genotype to

evaluate the process of CA1 degeneration for the group B mutants. The high variability of KA-induced excitotoxicity among the mutants could be due to the fact that the KA dose used, 20 mg/kg, is close to the threshold dose needed to evoke the clonic seizures (stage 3 seizure or more; supporting Fig. S1).

KA-evoked GABA release to generate gamma oscillations, preventing CA1 excitotoxicity

Systemic KA injection increases extracellular GABA levels in the rodent hippocampus (Zhang *et al.*, 1990; Ding *et al.*, 1998), which could be attributed to direct KA action on GluR5-containing KA receptors, which are located on presynaptic axon terminals of interneurons and release GABA (Khalilov *et al.*, 2002; Fisahn *et al.*, 2004). In the present study, KA injection into mutants did not increase GABA levels or trigger gamma oscillations in area CA1 in the same way as in control animals. However, it is possible that chronic reduction of afferent drives from area CA3 of mutants could result in KA-induced deficiencies in GABA release from CA1 interneurons. To rescue this deficit, we used DTX, a potent enhancer of presynaptic GABA release. DTX is a selective blocker of D-type voltage-gated potassium channels ($Kv_{1.1}$, $Kv_{1.2}$, and $Kv_{1.6}$) (Judge & Bever, 2006), and stimulates GABA release in rat cortical synaptosome fractions (Weller *et al.*, 1985), the rat entorhinal cortex (Cunningham & Jones, 2001), and the substantia nigra (Shimada *et al.*, 2007); the glutamate release activity seems to be weak in the rat hippocampus (Richards *et al.*, 2000) and the entorhinal cortex (Cunningham & Jones, 2001). As expected, administration of DTX prior to KA treatment restored the CA1 GABA levels in area CA1 but, remarkably, preserved KA-induced gamma oscillations. Released GABA, in turn, stimulates the $GABA_A$ receptors of other GABAergic cells and/or CA1 pyramidal cells, maintaining KA-triggered gamma oscillations (Bartos *et al.*, 2007; Mann & Paulsen, 2007). In fact, a recent study provides firm evidence that gamma oscillations arise from a network of mutually connected fast-spiking GABAergic neurons (Cardin *et al.*, 2009). Therefore, restoration of gamma oscillations in area CA1 by DTX treatment could be attributed to enhanced GABA release, regardless of DTX actions on other neurotransmitters. Interestingly, KA-induced extracellular secretion of the calcium-binding protein S100B from astrocytes has recently been shown to enhance KA-induced gamma oscillations (Sakatani *et al.*, 2008). Therefore, we cannot exclude the possibility that other mechanisms enhance the gamma oscillations upon KA administration.

Status epilepticus has long been implicated in brain damage, and several studies suggest a positive association between adverse outcomes and duration of status epilepticus (Norman, 1964; Corsellis & Bruton, 1983). In this study, we found that DTX pretreatment did not alter the magnitude of KA-induced seizure discharges, possibly due to the influence of enhanced SPW-R activity in the mutants. Therefore, KA-induced seizure severity during the first 2 h of status epilepticus did not necessarily determine the magnitude of excitotoxicity. In contrast, protection from excitotoxicity by pretreatment with DTX, accompanied by the re-emergence of persistent gamma oscillations, suggests that KA-induced GABA release is critical for the prevention of CA1 neurodegeneration. Furthermore, DTX pretreatment also significantly suppressed KA-induced epileptiform activity on the following day. This suggests that KA-induced GABA release which followed DTX pretreatment may prevent the initiation of subsequent processes leading to excitotoxicity, including epileptiform activity, on the following day (Fig. 11).

Clinical implications

What is most important in this study is that the magnitude of low-frequency gamma oscillations prior to the onset of behavioral seizures was inversely correlated with the occurrence of epileptiform activity on subsequent days (Fig. 10E). This is a finding of considerable clinical importance, because persistent gamma oscillations, which are measurable via electroencephalographic recordings in humans, could be used as an alternative prognostic indicator for predicting resilience to excitotoxicity. Interestingly, the prognostic value of oscillatory activity for seizure outcomes may vary with the oscillation frequencies. Fast gamma (60–100-Hz) oscillations have been reported to predict the development of ictal seizures in human neocortical epilepsy patients (Worrell *et al.*, 2004). In contrast, 'low-voltage fast activity' (> 13 Hz), beta frequency (15–30 Hz) or gamma frequency in the neocortex were more prevalent in favorable outcome groups after resective surgery (Lee *et al.*, 2000; Park *et al.*, 2002). The present findings suggest a good prognostic value of hippocampal low-frequency gamma oscillations, not only for prolonged epileptiform activity but also for excitotoxicity. Whether the identification of low-frequency gamma oscillations could be of prognostic value in the treatment of epilepsy patients remains unknown, but clearly warrants further research.

The use of cell-type-specific transgenic mutants also demonstrated that CA3 pyramidal cell-specific alterations are capable of initiating epilepsy after excitotoxic insults. It has long been suspected that the CA3 recurrent network is one of the critical loci in medial temporal lobe epilepsy (Buzsáki, 1986; Traub *et al.*, 1989). Recently, Nosten-Bertrand *et al.* (2008) reported that a dysplastic CA3 subfield in hippocampal slices of doublecortin KO mice generates SPW-like spontaneous activity and increases susceptibility to epilepsy. Interestingly, doublecortin mutations in humans cause type I lissencephaly to subcortical laminar heterotopia, which is associated with epilepsy (Guerrini & Marini, 2006). While it is unclear to what extent doublecortin mutation-derived defects are confined to the CA3 subfield in subcortical laminar heterotopia patients, the present study, along with these recent clinical data, suggest that the CA3 subfield may indeed be a site of epileptogenesis in humans.

Supporting information

Additional supporting information may be found in the online version of this article:

Fig. S1. Dose-response effect of KA treatment in fNR1 control mice.

Fig. S2. Region-specific neurodegeneration after KA treatment in CA3-NR1 KO mice.

Fig. S3. No NR1 ablation was detected in hippocampal GABAergic interneuron.

Please note: As a service to our authors and readers, this journal provides supporting information supplied by the authors. Such materials are peer-reviewed and may be re-organized for online delivery, but are not copy-edited or typeset by Wiley-Blackwell. Technical support issues arising from supporting information (other than missing files) should be addressed to the authors.

Acknowledgements

We thank Linus D. Sun and Catherine J. Cravens for technical assistance, Brian Condie and John Rubenstein for providing GAD67 cDNA plasmid, and György Buzsáki, Dax Hoffman, Karen N. Gale, Brita Fritsch, Kim Christian and Ioline Henter for valuable advice and critical reading of this manuscript. This research was supported by the Intramural Research Program of the

National Institute of Mental Health and by NIH Grant R01-MH078821 to S. Tonegawa. S. Jinde was supported, in part, by a Japan Society for the Promotion of Science (JSPS) fellowship.

Abbreviations

B6, C57BL/6; DG, dentate gyrus; DTX, α-dendrotoxin; fNR1, floxed-NR1; GABA, γ-aminobutyric acid; GAD67, 67-kDa isoform of glutamic acid decarboxylase; i.p., intraperitoneal; IR, immunoreactivity; KA, kainic acid; KO, knockout; LFP, local field potential; PBS, phosphate-buffered saline; SD, standard deviation; SPW, sharp wave; SPW-R, sharp wave–ripple.

References

Alarcon, G., Binnie, C.D., Elwes, R.D. & Polkey, C.E. (1995) Power spectrum and intracranial EEG patterns at seizure onset in partial epilepsy. *Electroencephalogr. Clin. Neurophysiol.*, **94**, 326–337.

Allen, P.J., Fish, D.R. & Smith, S.J. (1992) Very high-frequency rhythmic activity during SEEG suppression in frontal lobe epilepsy. *Electroencephalogr. Clin. Neurophysiol.*, **82**, 155–159.

Bartos, M., Vida, I. & Jonas, P. (2007) Synaptic mechanisms of synchronized gamma oscillations in inhibitory interneuron networks. *Nat. Rev. Neurosci.*, **8**, 45–56.

Behrens, C.J., van den Boom, L.P., de Hoz, L., Friedman, A. & Heinemann, U. (2005) Induction of sharp wave–ripple complexes in vitro and reorganization of hippocampal networks. *Nat. Neurosci.*, **8**, 1560–1567.

Ben-Ari, Y. (1985) Limbic seizure and brain damage produced by kainic acid: mechanisms and relevance to human temporal lobe epilepsy. *Neuroscience*, **14**, 375–403.

Ben-Ari, Y., Tremblay, E., Riche, D., Ghilini, G. & Naquet, R. (1981) Electrographic, clinical and pathological alterations following systemic administration of kainic acid, bicuculline or pentetrazole: metabolic mapping using the deoxyglucose method with special reference to the pathology of epilepsy. *Neuroscience*, **6**, 1361–1391.

Both, M., Bähner, F., von Bohlen und Halbach, O. & Draguhn, A. (2008) Propagation of specific network patterns through the mouse hippocampus. *Hippocampus*, **18**, 899–908.

Bragin, A., Engel, J. Jr, Wilson, C.L., Vizentin, E. & Mathern, G.W. (1999) Electrophysiologic analysis of a chronic seizure model after unilateral hippocampal KA injection. *Epilepsia*, **40**, 1210–1221.

Buzsáki, G. (1986) Hippocampal sharp waves: their origin and significance. *Brain Res.*, **398**, 242–252.

Buzsáki, G. & Draguhn, A. (2004) Neuronal oscillations in cortical networks. *Science*, **304**, 1926–1929.

Buzsáki, G., Buhl, D.L., Harris, K.D., Csicsvari, J., Czéh, B. & Morozov, A. (2003) Hippocampal network patterns of activity in the mouse. *Neuroscience*, **116**, 201–211.

Cardin, J.A., Carlén, M., Meletis, K., Knoblich, U., Zhang, F., Deisseroth, K., Tsai, LH. & Moore, C.I. (2009) Driving fast-spiking cells induces gamma rhythm and controls sensory responses. *Nature*, **459**, 663–667.

Chrobak, J.J. & Buzsáki, G. (1994) Selective activation of deep layer (V–VI) retrohippocampal cortical neurons during hippocampal sharp waves in the behaving rat. *J. Neurosci.*, **14**, 6160–6170.

Chrobak, J.J. & Buzsáki, G. (1996) High-frequency oscillations in the output networks of the hippocampal–entorhinal axis of the freely behaving rat. *J. Neurosci.*, **16**, 3056–3066.

Colgin, L.L., Kubota, D., Brucher, F.A., Jia, Y., Branyan, E., Gall, C.M. & Lynch, G. (2004) Spontaneous waves in the dentate gyrus of slices from the ventral hippocampus. *J. Neurophysiol.*, **92**, 3385–3398.

Corsellis, J.A. & Bruton, C.J. (1983) Neuropathology of status epilepticus in humans. *Adv. Neurol.*, **34**, 129–139.

Csicsvari, J., Hirase, H., Czurkó, A., Mamiya, A. & Buzsáki, G. (1999) Oscillatory coupling of hippocampal pyramidal cells and interneurons in the behaving Rat. *J. Neurosci.*, **19**, 274–287.

Csicsvari, J., Hirase, H., Mamiya, A. & Buzsáki, G. (2000) Ensemble patterns of hippocampal CA3–CA1 neurons during sharp wave-associated population events. *Neuron*, **28**, 585–594.

Cunningham, M.O. & Jones, R.S. (2001) Dendrotoxin sensitive potassium channels modulate GABA but not glutamate release in the rat entorhinal cortex in vitro. *Neuroscience*, **107**, 395–404.

Davies, J., Miller, A.J. & Sheardown, M.J. (1986) Amino acid receptor mediated excitatory synaptic transmission in the cat red nucleus. *J. Physiol.*, **376**, 13–29.

Ding, R.G., Asada, H. & Obata, K. (1998) Changes in extracellular glutamate and GABA levels in the hippocampal CA3 and CA1 areas and the induction of glutamic acid decarboxylase-67 in dentate granule cells of rats treated with kainic acid. *Brain Res.*, **800**, 105–110.

Fernández de Sevilla, D., Garduño, J., Galván, E. & Buño, W. (2006) Calcium-activated afterhyperpolarizations regulate synchronization and timing of epileptiform bursts in hippocampal CA3 pyramidal neurons. *J. Neurophysiol.*, **96**, 3028–3041.

Fisahn, A., Contractor, A., Traub, R.D., Buhl, E.H., Heinemann, S.F. & McBain, C.J. (2004) Distinct roles for the kainate receptor subunits GluR5 & GluR6 in kainate-induced hippocampal gamma oscillations. *J. Neurosci.*, **24**, 9658–9668.

Fisher, R.S., Webber, W.R., Lesser, R.P., Arroyo, S. & Uematsu, S. (1992) High-frequency EEG activity at the start of seizures. *J. Clin. Neurophysiol.*, **9**, 441–448.

Freund, T.F. & Buzsáki, G. (1996) Interneurons of the hippocampus. *Hippocampus*, **6**, 347–470.

Guerrini, R. & Marini, C. (2006) Genetic malformations of cortical development. *Exp. Brain Res.*, **173**, 322–333.

Hirase, H., Leinekugel, X., Csicsvari, J., Czurkó, A. & Buzsáki, G. (2001) Behavior-dependent states of the hippocampal network affect functional clustering of neurons. *J. Neurosci.*, **21**, 1–4.

Hughes, J.R. (2008) Gamma, fast, and ultrafast waves of the brain: their relationships with epilepsy and behavior. *Epilepsy Behav.*, **13**, 25–31.

Jirsch, J.D., Urrestarazu, E., LeVan, P., Olivier, A., Dubeau, F. & Gotman, J. (2006) High-frequency oscillations during human focal seizures. *Brain*, **129**, 1593–1608.

Judge, S.I. & Bever, C.T. Jr (2006) Potassium channel blockers in multiple sclerosis: neuronal Kv channels and effects of symptomatic treatment. *Pharmacol. Ther.*, **111**, 224–259.

Kemp, J.A. & Sillito, A.M. (1982) The nature of the excitatory transmitter mediating X and Y cell inputs to the cat dorsal lateral geniculate nucleus. *J. Physiol.*, **323**, 377–391.

Khalilov, I., Hirsch, J., Cossart, R. & Ben-Ari, Y. (2002) Paradoxical anti-epileptic effects of a GluR5 agonist of kainate receptors. *J. Neurophysiol.*, **88**, 523–527.

Khazipov, R. & Holmes, G.L. (2003) Synchronization of kainate-induced epileptic activity via GABAergic inhibition in the superfused rat hippocampus in vivo. *J. Neurosci.*, **23**, 5337–5341.

Klausberger, T. & Somogyi, P. (2008) Neuronal diversity and temporal dynamics: the unity of hippocampal circuit operations. *Science*, **321**, 53–57.

Lee, S.A., Spencer, D.D. & Spencer, S.S. (2000) Intracranial EEG seizure-onset patterns in neocortical epilepsy. *Epilepsia*, **41**, 297–307.

Maier, N., Nimmrich, V. & Draguhn, A. (2003) Cellular and network mechanisms underlying spontaneous sharp wave–ripple complexes in mouse hippocampal slices. *J. Physiol.*, **550**, 873–887.

Mann, E.O. & Paulsen, O. (2007) Role of GABAergic inhibition in hippocampal network oscillations. *Trends Neurosci.*, **30**, 343–349.

McHugh, T.J., Blum, K.I., Tsien, J.Z., Tonegawa, S. & Wilson, M.A. (1996) Impaired hippocampal representation of space in CA1-specific NMDAR1 knockout mice. *Cell*, **87**, 1339–1349.

McKhann, G.M., Wenzel, H.J., Robbins, C.A., Sosunov, A.A. & Schwartzkroin, P.A. (2003) Mouse strain differences in kainic acid sensitivity, seizure behavior, mortality, and hippocampal pathology. *Neuroscience*, **122**, 551–561.

McLin, J.P. & Steward, O. (2006) Comparison of seizure phenotype and neurodegeneration induced by systemic kainic acid in inbred, outbred, and hybrid mouse strains. *Eur. J. Neurosci.*, **24**, 2191–2202.

Medvedev, A.V. (2001) Temporal binding at gamma frequencies in the brain: paving the way to epilepsy? *Australas. Phys. Eng. Sci. Med.*, **24**, 37–48.

Medvedev, A., Mackenzie, L., Hiscock, J.J. & Willoughby, J.O. (2000) Kainic acid induces distinct types of epileptiform discharge with differential involvement of hippocampus and neocortex. *Brain Res. Bull.*, **52**, 89–98.

Miller, K.D., Chapman, B. & Stryker, M.P. (1989) Visual responses in adult cat visual cortex depend on N-methyl-D-aspartate receptors. *Proc. Natl Acad. Sci. USA*, **86**, 5183–5187.

Mody, I. (1998) Ion channels in epilepsy. *Annu. Rev. Pharmacol. Toxicol.*, **38**, 321–350.

Nadler, J.V. (1981) Minireview. Kainic acid as a tool for the study of temporal lobe epilepsy. *Life Sci.*, **29**, 2031–2042.

Nakazawa, K., Quirk, M.C., Chitwood, R.A., Watanabe, M., Yeckel, M.F., Sun, L.D., Kato, A., Carr, C.A., Johnston, D., Wilson, M.A. & Tonegawa, S. (2002) Requirement for hippocampal CA3 NMDA receptors in associative memory recall. *Science*, **297**, 211–218.

Nakazawa, K., Sun, L.D., Quirk, M.C., Rondi-Reig, L., Wilson, M.A. & Tonegawa, S. (2003) Hippocampal CA3 NMDA receptors are crucial for memory acquisition of one-time experience. *Neuron*, **38**, 305–315.

Norman, R.N. (1964) The neuropathology of status epilepticus. *Med. Sci. Law*, **4**, 45–61.

Nosten-Bertrand, M., Kappeler, C., Dinocourt, C., Denis, C., Germain, J., Phan Dinh Tuy, F., Verstraeten, S., Alvarez, C., Métin, C., Chelly, J., Giros, B., Miles, R., Depaulis, A. & Francis, F. (2008) Epilepsy in Dcx knockout mice associated with discrete lamination defects and enhanced excitability in the hippocampus. *PLoS ONE*, **3**, e2473.

Papatheodoropoulos, C. & Kostopoulos, G. (2002) Spontaneous GABA(A)-dependent synchronous periodic activity in adult rat ventral hippocampal slices. *Neurosci. Lett.*, **319**, 17–20.

Park, S.A., Lim, S.R., Kim, G.S., Heo, K., Park, S.C., Chang, J.W., Chung, S.S., Choi, J.U., Kim, T.S. & Lee, B.I. (2002) Ictal electrocorticographic findings related with surgical outcomes in nonlesional neocortical epilepsy. *Epilepsy Res.*, **48**, 199–206.

Prince, D.A. (1978) Neurophysiology of epilepsy. *Annu. Rev. Neurosci.*, **1**, 395–415.

Pulsinelli, W.A., Brierley, J.B. & Plum, F. (1982) Temporal profile of neuronal damage in a model of transient forebrain ischemia. *Ann. Neurol.*, **11**, 491–498.

Racine, R.J. (1972) Modification of seizure activity by electrical stimulation. II. Motor seizure. *Electroencephalogr. Clin. Neurophysiol.*, **32**, 281–294.

Ramakers, G.J., Corner, M.A. & Habets, A.M. (1990) Development in the absence of spontaneous bioelectric activity results in increased stereotyped burst firing in cultures of dissociated cerebral cortex. *Exp. Brain Res.*, **79**, 157–166.

Richards, D.A., Morrone, L.A., Bagetta, G. & Bowery, N.G. (2000) Effects of alpha-dendrotoxin and dendrotoxin K on extracellular excitatory amino acids and on electroencephalograph spectral power in the hippocampus of anaesthetised rats. *Neurosci. Lett.*, **293**, 183–186.

Sakatani, S., Seto-Ohshima, A., Shinohara, Y., Yamamoto, Y., Yamamoto, H., Itohara, S. & Hirase, H. (2008) Neural-activity-dependent release of S100B from astrocytes enhances kainate-induced gamma oscillations in vivo. *J. Neurosci.*, **28**, 10928–10936.

Salt, T.E. (1986) Mediation of thalamic sensory input by both NMDA receptors and non-NMDA receptors. *Nature*, **322**, 263–265.

Schauwecker, P.E. & Steward, O. (1997) Genetic determinants of susceptibility to excitotoxic cell death: implications for gene targeting approaches. *Proc. Natl Acad. Sci. USA*, **94**, 4103–4108.

Schmued, L.C. & Hopkins, K.J. (2000) Fluoro-Jade B: a high affinity fluorescent marker for the localization of neuronal degeneration. *Brain Res.*, **874**, 123–130.

Schwob, J.E., Fuller, T., Price, J.L. & Olney, J.W. (1980) Widespread patterns of neuronal damage following systemic or intracerebral injections of kainic acid: a histological study. *Neuroscience*, **5**, 991–1014.

Shimada, H., Uta, D., Nabekura, J. & Yoshimura, M. (2007) Involvement of Kv channel subtypes on GABA release in mechanically dissociated neurons from the rat substantia nigra. *Brain Res.*, **1141**, 74–83.

Silveira, R., Siciliano, J., Abo, V., Viera, L. & Dajas, F. (1988) Intrastriatal dendrotoxin injection: behavioral and neurochemical effects. *Toxicon*, **26**, 1009–1015.

Simpson, M.T., MacLaurin, J.G., Xu, D., Ferguson, K.L., Vanderluit, J.L., Davoli, M.A., Roy, S., Nicholson, D.W., Robertson, G.S., Park, D.S. & Slack, R.S. (2001) Caspase 3 deficiency rescues peripheral nervous system defect in retinoblastoma nullizygous mice. *J. Neurosci.*, **21**, 7089–7098.

Singer, W. & Gray, C.M. (1995) Visual feature integration and the temporal correlation hypothesis. *Annu. Rev. Neurosci.*, **18**, 555–586.

Sperk, G. (1994) Kainic acid seizures in the rat. *Prog. Neurobiol.*, **42**, 1–32.

Trasande, C.A. & Ramirez, J.M. (2007) Activity deprivation leads to seizures in hippocampal slice cultures: is epilepsy the consequence of homeostatic plasticity? *J. Clin. Neurophysiol.*, **24**, 154–164.

Traub, R.D. & Wong, K. (1982) Cellular mechanism of neuronal synchronization in epilepsy. *Science*, **216**, 745–747.

Traub, R.D., Miles, R. & Wong, R.K.S. (1989) Model of the origin of rhythmic population oscillations in the hippocampal slice. *Science*, **242**, 1319–1325.

Traub, R.D., Jefferys, J.G.R. & Whittington, M. (1999) *Fast Oscillations in Cortical Circuits*. MIT Press, Cambridge, MA.

Uhlhaas, P.J. & Singer, W. (2006) Neural synchrony in brain disorders: relevance for cognitive dysfunctions and pathophysiology. *Neuron*, **52**, 155–168.

Weller, U., Bernhardt, U., Siemen, D., Dreyer, F., Vogel, W. & Habermann, E. (1985) Electrophysiological and neurobiochemical evidence for the blockade of a potassium channel by dendrotoxin. *Naunyn Schmiedebergs Arch. Pharmacol.*, **330**, 77–83.

Whittington, M.A., Traub, R.D. & Jefferys, J.G. (1995) Synchronized oscillations in interneuron networks driven by metabotropic glutamate receptor activation. *Nature*, **373**, 612–615.

Wilson, M.A. & McNaughton, B.L. (1993) Dynamics of the hippocampal ensemble code for space. *Science*, **261**, 1055–1058.

Worrell, G.A., Parish, L., Cranstoun, S.D., Jonas, R., Baltuch, G. & Litt, B. (2004) High-frequency oscillations and seizure generation in neocortical epilepsy. *Brain*, **127**, 1496–1506.

Ylinen, A.M., Miettinen, R., Pitkänen, A., Gulyas, A.I., Freund, T.F. & Riekkinen, P.J. (1991) Enhanced GABAergic inhibition preserves hippocampal structure and function in a model of epilepsy. *Proc. Natl Acad. Sci. USA*, **88**, 7650–7653.

Zhang, W.Q., Rogers, B.C., Tandon, P., Hudson, P.M., Sobotka, T.J., Hong, J.S. & Tilson, H.A. (1990) Systemic administration of kainic acid increases GABA levels in perfusate from the hippocampus of rats in vivo. *Neurotoxicology*, **11**, 593–600.

Zhao, M., Adams, J.P. & Dudek, S.M. (2005) Pattern-dependent role of NMDA receptors in action potential generation: consequences on extracellular signal-regulated kinase activation. *J. Neurosci.*, **25**, 7032–7039.